Distribution Agreement

In presenting this thesis as a partial fulfillment of the requirements for a degree from Emory University, I hereby grant to Emory University and its agents the non-exclusive license to archive, make accessible, and display my thesis in whole or in part in all forms of media, now or hereafter know, including display on the World Wide Web. I understand that I may select some access restrictions as part of the online submission of this thesis. I retain all ownership rights to the copyright of the thesis. I also retain the right to use in future works (such as articles or books) all or part of this thesis.

Charles Qi March 30, 2022

Polariton mediated reservoir energy transfer in disordered photonic wires

By

Charles Qi

Dr. Raphael F. Ribeiro

Advisor

Chemistry

Dr. Raphael F. Ribeiro

Advisor

Dr. James T. Kindt

Committee Member

Dr. Fang Liu

Committee Member

2022

Polariton mediated reservoir energy transfer

in disordered photonic wires

By

Charles Qi

Dr. Raphael F. Ribeiro

Advisor

An abstract of
a thesis submitted to the Faculty of Emory College of Arts and Sciences
of Emory University in partial fulfillment
of the requirements of the degree of
Bachelor of Science with Honors

Chemistry

2022

Abstract

Strong light-matter interactions are emerging as an innovative way to modify chemical reactions and promote changes in molecular systems. One function of strong light-matter interactions that is still not fully understood is their ability to facilitate efficient and effective intermolecular energy transfer beyond the Förster limit. This work aims to build computational models that represent quantum systems within Fabry-Perot cavities to gain insight into the mechanisms behind polariton-mediated energy transfer and the conditions that maximize its efficiency. Unlike previous works, stochastic fluctuations of the transition energies of molecules within the system were incorporated. Results show a greater than 50% decrease in effectiveness of energy transfer when the energy of the cavity is raised to higher than the molecular transition energies. Results also show a 10-fold increase in the effectiveness of energy transfer when energetic disorder is increased from a standard deviation of 0 eV to 0.13 eV in a Gaussian distribution. Conclusions from this work provide additional insight into some puzzling experimental results, but more complex models will likely be required to gain complete understanding of experimental observations.

Polariton mediated reservoir energy transfer in disordered photonic wires

By

Charles Qi

Dr. Raphael F. Ribeiro

Advisor

A thesis submitted to the Faculty of Emory College of Arts and Sciences
of Emory University in partial fulfillment
of the requirements of the degree of
Bachelor of Science with Honors

Chemistry

2022

Acknowledgements

I would like to acknowledge Dr. Ribeiro for advising me through my research. He has guided me through the work and helped me develop my research for the past year. I would also like to acknowledge Dr. James Kindt for bringing up interesting comments during my research and Dr. Fang Liu for being my professor for all Quantum Mechanics classes I took during my undergraduate time at Emory.

I would like to thank my parents for supporting me throughout my undergraduate career. Without them, I would not have been able to gain the education needed to create this work. My father's previous history in physics drove me to generate this work, while my mother's constant support has brought out all my hard work out during this research. This work thus stands as evidence of what I can achieve with their full support and belief in me.

Table of Contents

List of Tables and Figures

List of Supplementary Materials

1. Introduction

Light has been a tool in chemistry used to understand molecular processes and initiate chemical reactions. In most cases, however, light only has a weak interaction with molecules, known as weak coupling. This weak coupling allows for short-lived changes in quantum states, a necessary change for spectrometry and photochemical dynamics [1].

Over the last decade, increasing amounts of interest has been grown regarding strong coupling regimes, in which the rate of the molecules exchanging energy in the form of light is faster than the rate at which the molecules exchange energy with their environment [2]. This phenomenon, known as strong light-matter coupling, occurs within Fabry-Perot cavities that use constructive interference to generate high powered light that can interact with the molecules inside [3]. Research in this field has led to new ways of controlling regioselectivity in chemical reactions and provides an easier pathway for reverse intersystem crossing [4] [5] [6].

1.1 Fabry-Perot Cavities

Fabry-Perot cavities are used to create strong coupling regimes. These cavities are made by two semi reflective mirrors placed in close proximity to each other, usually on the order of micrometers [7]. Because the mirrors are only semi reflective, if light is shone onto the cavity, some of the light can pass through the first mirror and enter the cavity. The light will then reflect off the second mirror and stay between the two mirrors inside the cavity until it passes through the second semi reflective mirror to be detected by instruments.

If light is shone directly onto the mirror with an incidence angle of 0 degrees, interesting results occur when the distance between the two mirrors is equal to an integer number times ½ of the wavelength of the light shone on it [8]. This happens because when $L = n\frac{\lambda}{2}$, L being the length of the cavity and n being a positive integer, the phase factor representing the change in

phase of the light after being reflected off the mirrors equals to 1 and can be removed from many equations. When this requirement is satisfied, the cavity and the light are said to be in phase, and the cavity is excited to a "cavity mode" [9]

Figure 1a shows an example of a cavity. As seen in the figure, light entering the mirrors creates a standing wave with quantized cavity modes.

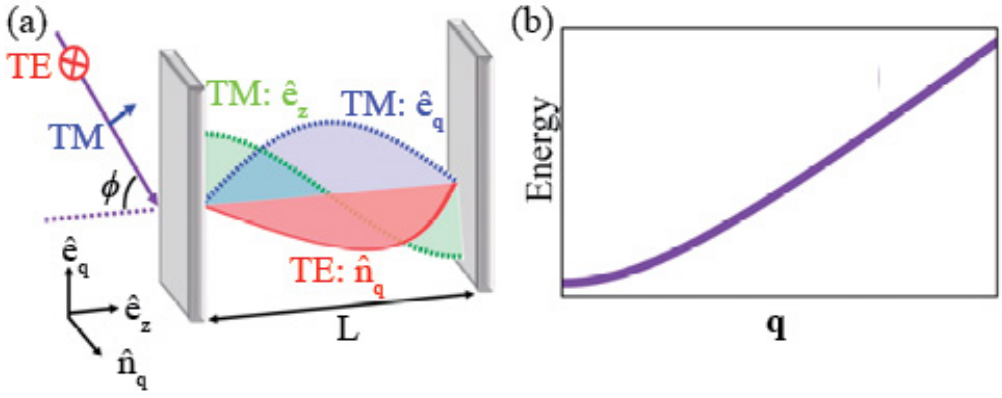

Figure 1. (a) Representation of a Fabry-Perot cavity. ϕ represents the incidence angle of the light shining on the cavity. Both transverse magnetic (TM) and transverse electric (TE) polarizations of light are shown. (b) Energy of the cavity as a function of the in-plane wave vector **q**, known as a dispersion plot (Adapted from Ref [10]).

Figure 1b represents the energy of the cavity as a function of in-plane wave vector (dispersion plot). Because this in-plane wave vector is directly related to the angle of incidence of the laser (ϕ in Figure 1a), some papers show the dispersion plot by the energy of the cavity as a function of angle of incidence [11] [12]. Equation 1 governs the trend in the dispersion plot in an empty cavity.

$$\omega_{q,m} = c\sqrt{q^2 + (\frac{m\pi}{L})^2}$$

Equation 1

In Equation 1, L represents the length of the cavity while m is the quantum number of the cavity mode.

1.2 Strong Light-Matter Coupling Within Cavities

Strong coupling of molecules with light occurs when the rate at which energy is transferred between light and molecules in the cavity is considerably larger than both the rate at which light leaves the cavity and the dephasing rate after the molecules are perturbed by the cavity photons [13]. When strong coupling occurs, the molecules and the cavity become quantumly entangled and generate quantum states that are linear combinations of both the molecules and the cavity photons. These hybrid light-matter states, known as polaritonic states, have energies and lifetimes that are significantly different from the energies and lifetimes measured when the molecules are excited outside of a cavity [14].

Measuring the absorption spectrum of a strongly coupled system shows that the absorption frequencies of these polaritonic states are very different from the absorption frequencies of the original molecules [15]. Figure 2a shows a pictorial representation of the generation of two new polaritonic states when a molecular emitter and a cavity photon are strongly coupled. These two new polaritonic states can be named Upper Polariton (UP) and Lower Polariton (LP), with the UP being higher in energy than the LP [16].

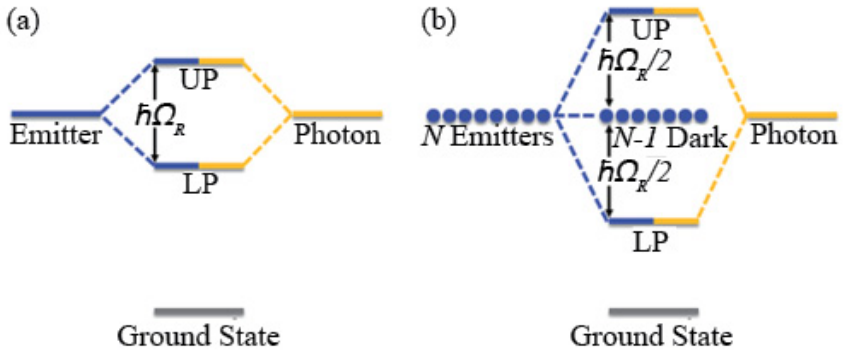

Figure 2. (a) Energies of the molecular emitter, a single photon within the cavity, and the UP and LP states. UP and LP states are created once the molecule and the photon are strongly coupled. They have both photonic and molecular contents, as shown by the yellow and blue colors combining to make up the UP and LP bands. (b) A new set of dark modes with *N-1* states is shown when multiple molecular emitters are strongly coupled with a photon within the cavity. The dark states have no photonic content in this idealized model due to its weak interaction with the cavity. This is shown by the dark states being only blue. Ω_R represents the strength of the light-matter interaction, known as the Rabi splitting (Adapted from Ref [10]).

When multiple molecular emitters are coupled to the cavity, a new set of dark modes are formed in addition to the UP and the LP states [17] [18]. This is seen in Figure 2b, where *N* is the number of emitters coupled to one cavity photon, yielding one UP, one LP, and *N-1* dark states. The dark states retain the original emitter's energy due to their lack of strong coupling with light and have only molecular characteristics in this idealized model [19]. They are important when considering the dynamics of the system.

The strength of the light-matter interaction is known as the Rabi splitting (Ω_R). In Figure 2a, the energy gap between the UP and the LP represents the Rabi splitting, while in Figure 2b, the energy gap between the UP and the dark states (along with the dark states and the LP) represent half the Rabi splitting [20].

The dispersion plots for strongly coupled systems show the combination of the molecular excitons (excited states) with the cavity photons to make the UP and the LP (Figure 3b). The shortest energy gap at a fixed wave vector between the UP and the LP bands represents the Rabi splitting [2]. The Rabi splitting is proportional to the square root of the density of emitters multiplied by the average dipole moment of the emitters [21].

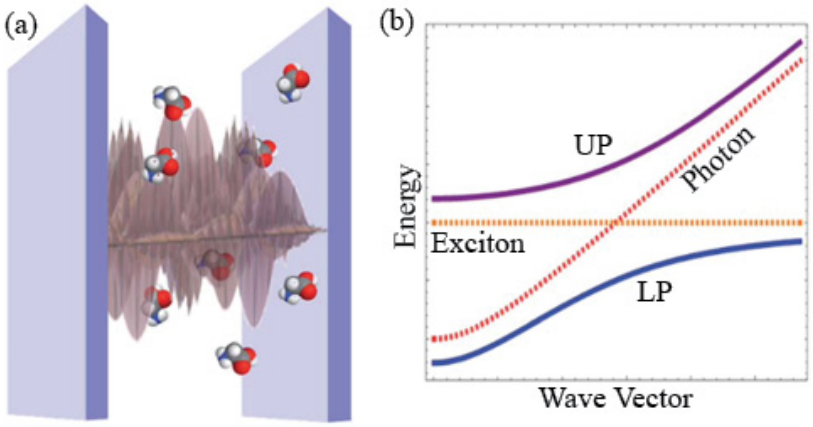

Figure 3. (a) Pictorial representation of a cavity with molecules strongly coupled within. (b) Dispersion plot (energy as a function of in-plane wave vector) of the energies of the new polaritonic states generated when the exciton strongly couples with the photon (Adapted from Ref [10]).

Just as in Figure 1b, the dispersion graph can also be shown as the energy as a function of incidence angle of the laser.

1.3. Energy Transfer within Strong Coupling Regime

Cavities can also be strongly coupled to two different types of molecular excitons with different excitation energies. When this occurs, energy can be transferred between the two different types of molecules at further distances and at much quicker rates. In fact, experiments have seen a distance independent relationship between the two different types of molecules when they transfer energy under a strong coupling regime [22].

This result is notable because energy transfer generally occurs via short-range Förster resonance energy transfer (FRET) [23]. In FRET, the rate of energy transfer between molecules is proportional to $1/R_{DA}^{6}$, where R_{DA} is the average distance between the donor and the acceptor molecules [24]. With this relationship, any energy transfer between molecules becomes highly unlikely at distances greater than 10 nm. Furthermore, the energy emitted by the donor must be relatively equal to the excitation energy of the acceptor [25]. Experiments using strong coupling regimes have obtained results that support the regime's ability to facilitate efficient energy transfer beyond the Förster limit [22] [26].

This phenomenon of efficient energy transfer is reasonably understood and can be ascribed to the thermal bias towards lower-energy excitations that can be accessed by polaritons [10] [27]. However, more recent work has established intermolecular energy transfer in situations with minimal thermal bias, such as vibrational transitions as opposed to electronic exciton transitions [28] [29]. Thus, the mechanism discussed in Ref [27] may be irrelevant. This suggests that another mechanism is operative under conditions of vibrational strong coupling. Estimates of intermolecular energy transfer between off-resonant vibrational modes using idealized models (as in Ref [30]) in fact give much slower transport than observed experimentally (by orders of magnitude). This poses a major challenge to our understanding of these processes.

1.4. Statement of Purpose

The present work focuses on examining computational models that represent strong coupling systems and gain insight into the mechanism at which energy is transferred from donor to acceptor molecules within strong coupling regimes. Additionally, the present work

investigates how considering disorder within strong coupling regimes can help create models that help elucidate recent puzzling experimental observations in the field.

2. Computational Model

This work modeled a cavity that is strongly coupled to two different types of molecules: a donor and an acceptor molecule. The molecules were assumed to only have one ground state and one excited state, and thus only have one excitation energy. The model utilized a simplified version of a cavity. Instead of treating the molecules within the cavity to be freely moving within a three-dimensional space, this model treated the molecules to be distributed on a one-dimensional line. This type of cavity can be thought of as a photonic wire, as shown in Figure 4.

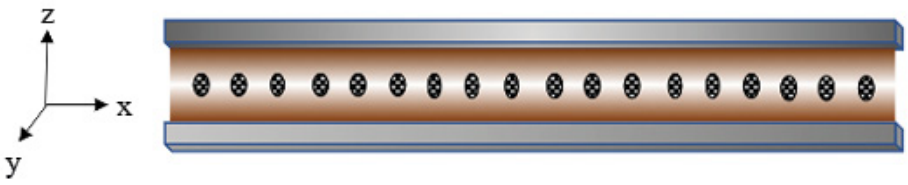

Figure 4. Model of photonic wire used to represent cavity system. Adapted from Ref [31].

This photonic wire model places molecules in a one-dimensional uniform lattice, thus simplifying the Hamiltonian calculations. Similar photonic wires have also been achieved experimentally [32].

The geometry of the wire was made into the shape of a ring, where the first molecule and the last molecule in the lattice are neighboring each other. This removed complications relating to dynamics of molecules at the end of the lattice. Having this configuration was justified in models with many molecules. This is because in experiments investigating exciton coupling within photonic wires, a large number of molecules is generally involved (10^6 or higher) [33]. Thus, edge or surface effects become irrelevant, as the number of molecules at the "ends" are small compared to the number of molecules within the bulk.

Some disorder was introduced to make the photonic wire model more realistic. When placing the molecules into the photonic wire, the positions of the molecules could have been simplified by either alternating between donor and acceptor molecules or placing all donor molecules on one half of the wire and all acceptor molecules on the other. However, this would have been too idealistic; thus, the positions of the donor and acceptor molecules within the wire were randomized.

The excitation energies of the molecules were set to assimilate organic electronic transitions. The donor molecule had an excitation energy of 2.4 eV while the acceptor molecule had an excitation energy of 2.1 eV. The choice of electronic excitations over vibrational excitations was due to the larger number of molecules generally involved in vibrational strong coupling (See Supplementary Materials Section S1 for further explanation).

Equation 2 shows an example Hamiltonian matrix for a system with two cavity modes, two donor (*D*) molecules, and two acceptor (*A*) molecules [31].

$$H = \begin{pmatrix} E_{C1} & 0 & I(0,0) & I(0,1) & I(0,2) & I(0,3) \\ 0 & E_{C2} & I(1,0) & I(1,1) & I(1,2) & I(1,3) \\ I^*(0,0) & I^*(1,0) & E_{D1} & 0 & 0 & 0 \\ I^*(0,1) & I^*(1,1) & 0 & E_{D2} & 0 & 0 \\ I^*(0,2) & I^*(1,2) & 0 & 0 & E_{A1} & 0 \\ I^*(0,3) & I^*(1,3) & 0 & 0 & 0 & E_{A2} \end{pmatrix}$$

Equation 2

As shown in Equation 2, E_i represents either the energy of a donor molecule, acceptor molecule, or a cavity photon. *I(i,k)* represents the interaction of light and matter between cavity photon *i* and molecule *k*, with *I*(i,k)* representing the complex conjugate.

Equation 3 gives the light-matter interaction – *I(i,k)* [31].

$$I(i,k) = \frac{1}{2}\Omega_{D,A}\sqrt{E_{D,A}/(Nmol * E_{Ci})}e^{iq_{ci}x_k}$$

Equation 3

As shown in Equation 3, $\Omega_{D,A}$ represents the Rabi splitting for each molecule (*D* or *A*), $E_{D,A}$ represents the excited state energy of the molecule (*D* or *A*), E_{Ci} represents the energy of the cavity photon *i*, *Nmol* represents the number of molecules within the system, q_i represents the magnitude of the cavity photon in-plane wave vector in the x direction (see Fig. 4), and x_k represents the position of molecule *k* in the cavity. With the model cavity being in a ring geometry, q_{ci} contains photonic momentum for both clockwise and counterclockwise motion (positive and negative respectively), along with a photon with 0 in-plane momentum.

The energy of the cavity photons was calculated based on the size of the photonic wire cavity system. Equation 4 represents how the energy of the cavity photons were calculated from the in-plane momentum of the photons in the system [31].

$$E_c = \frac{\hbar c}{\sqrt{3}}\sqrt{q_z^2 + q_y^2}\sqrt{1 + q_{ci}^2/\sqrt{q_z^2 + q_y^2}}$$

Equation 4

In equation 4, $\hbar$ is in units of *eV•s*, the speed of light is in *m/s,* and the square root of 3 represents the refractive index of the medium within the cavity. The terms q_z and q_y represent the quantized wave vectors in the z and y direction respectively, with both assumed to be in the ground state.

Using both equations 2 and 3, model Hamiltonians can be generated for many systems, and the diagonalization of the Hamiltonians can lead to observables that can be compared to experimental results.

2.1. Closed System Quantum Dynamics

Infinite-Time dynamics represent observables that occur within fully quantum-mechanical closed systems. With no exchange of energy between the cavity system and the environment, all the energy stays within the system, thus constituting closed system dynamics. The transfer of energy between molecules can be quantified as the probability that the energy found in a donor molecule will end up in an acceptor molecule after a very long time. This probability, denoted as P_{DA}, can be calculated by multiplying the absolute value squared of the probability amplitudes of the donor and acceptor basis states, then summing over all possible eigenstates (Eq. 5) [31].

$$P_{DA}(t \to \infty) = \sum_{\alpha} |c_{D\alpha}|^2 |c_{\alpha A}|^2$$

Equation 5

As shown in equation 5, $c_{D\alpha}$ represents the coefficients that come from the linear combination of donor states *D* for each eigenstate α. This probability (known as transition probability) can be calculated for many different systems and used as a source for comparison between systems with different conditions.

2.2. Open Quantum System Dynamics via Pauli Master Equation

While the closed system model is useful to obtain a sense of difference between idealized models and disordered models, it is ultimately unrealistic, because energy must leak from the cavity system for spectroscopic instruments to detect signatures [34]. Thus, open quantum system dynamics consider the leakage of photons through the cavity mirrors and the possibility of excited polaritons or molecules to decay to the ground state and release energy in the form of heat to the surroundings [35] [36]. The system is thus considered to be in contact with a thermal bath that collects the heat released by the decaying molecules and that acts as a medium for

energy transfer between molecules [37]. The thermal bath plays a role when any higher energy state decays into a lower energy state, since any excess energy is transferred directly to the thermal bath. Additionally, any energy required to move to a higher energy state could be taken from the thermal bath.

These transfer processes are incorporated into the model using rate constants derived from the eigenstates of the closed-system Hamiltonian. The transition rates between two states α and β are obtained through perturbation theory and Fermi's Golden Rule (Eq. 6) [38].

$$k_{\alpha\to\beta} = \frac{2\pi}{\hbar}\sum_{m} P_{m\alpha}P_{m\beta}W(E_\beta - E_\alpha)$$

Equation 6

In equation 6, $P_{m\alpha}$ represents the probability of molecule m to be detected in the excited state when the system is in eigenstate α. $W(E_\beta - E_\alpha)$ is a rate factor extracted from the absorption spectrum of the molecules outside of a cavity [39] [40].

As stated in Section 1.3, experimental results occurring under conditions of minimal thermal bias are still not understood. Thus, to investigate these conditions, thermal bias was removed by keeping W constant for all transitions. This meant that transitioning from state α to state β would have the same rate constant as transitioning from state β to state α.

Absence of thermal bias is equivalent to assuming that the difference in excitation energies between the molecules is much smaller than k_BT. With excitation energies of donor and acceptor molecules assimilating electronic transitions, the temperature of such an experiment would be high for entropy to dominate over the kinetics of the system [41].

Photon leakage and molecular excited-state population relaxation kinetics were incorporated through equation 7.

$$k_{\alpha\to G} = \kappa \sum_{q=0}^{N_q-1} P_{q\alpha} + \Gamma_D \sum_{m_D=0}^{N_D-1} P_{m_D\alpha} + \Gamma_A \sum_{m_A=0}^{N_A-1} P_{m_A\alpha}$$

Equation 7

In equation 7, κ represents the lifetimes for a photon to leak through the mirrors of the cavity, while Γ_D and Γ_A represent the lifetimes for donor and acceptor molecules to decay and release heat into the thermal bath respectively; q represents the specific photonic mode, m_D represents the donor molecular mode, and m_A represents the acceptor molecular mode. The photonic leakage rate (κ) was set at $3x10^{13}$ *1/s*, while the molecular thermal relaxation rates (Γ_D and Γ_A) were set at $1x10^{9}$ *1/s* [42].

Using all these rate equations, a set of coupled differential equation can be used that governs the evolution of the open quantum system through time (Eq. 8) [43].

$$\frac{d\boldsymbol{P}}{dt} = \mathrm{K}\boldsymbol{P}(\boldsymbol{t})$$

Equation 8

In equation 8, the vector ***P*** contains the probability that an excitation is found in a specific eigenstate. The differential equation thus provides the model with the evolution of this vector ***P*** as a function of time. *K* is the transition matrix containing all the rate constants calculated in equations 6 and 7. This transition matrix is generated by equations 9 and 10.

$$K_{\alpha\alpha} = -\sum_{\beta\neq\alpha} k_{\alpha\to\beta} - k_{\alpha\to G}$$

Equation 9

$$K_{\alpha\beta} = k_{\beta\to\alpha}, \beta \neq \alpha$$

Equation 10

As shown in equations 9 and 10, the diagonal matrix elements of the K matrix represent the decay rates for each eigenstate, while the off-diagonal matrix elements represent the transition rates between two states. Thus, all diagonal elements of the matrix were negative while all off-diagonal matrix elements were positive, leading to only negative eigenvalues that enforce an exponential decay trend for all probabilities [44].

Once the rate calculations are set up, an initial vector $\boldsymbol{P}$ can be chosen, and the differential equation can be solved. The solution can then be used to show the evolution of the system over time.

3. Closed System Quantum Dynamics

3.1. Ideal Model

Using the equations outlined in section 2, a Hamiltonian can be generated to model an ideal case of the photonic wire cavity. The ideal system contained 250 donor molecules and 250 acceptor molecules. This number of molecules was chosen to fit the photonic wire model. The transition probabilities scaled in an approximately $1/N$ fashion (See Supplementary Section S2). However, this particular number of molecules was chosen since they gave rise to large length scales at around 5 to 20 micrometers on the x direction (see Figure 4). This allowed the cavity to fully confine all molecules on a line to follow a photonic wire geometry while keeping computational costs low [45].

The ideal system contained 251 photonic modes that were split up into 125 modes traveling clockwise in the ring geometry with a positive wave vector, 125 modes traveling counterclockwise with a negative wave vector, and one mode with a 0-momentum wave vector. Only near resonant photonic modes are relevant since higher energy photon modes do not strongly couple with the molecules to form polaritons [46]. This number of photon modes was

chosen to ensure that all conditions contained enough near resonant photon modes to ensure proper dynamics.

With this case being the ideal model, there were no deviations in excitation energy, thus all donor molecules had an excitation energy of 2.4 and all acceptor molecules had an excitation energy of 2.1. The Rabi splitting was set at 0.3 eV.

The lowest energy photon mode was set to be under the excitation energies of both the donor and acceptor molecules. Thus, the cavity was made to be 200 nm in the z direction and 400 nm in the y direction, making the lowest energy photon mode to be approximately 2.0 eV with both z and y quantum numbers being 1. The distance between the molecules was set at 20 nm, making this 500-molecule system having a length of 10 μm in the x direction.

Figure 5 shows the dispersion plot along with the energies of the photons and the molecules of this ideal cavity system.

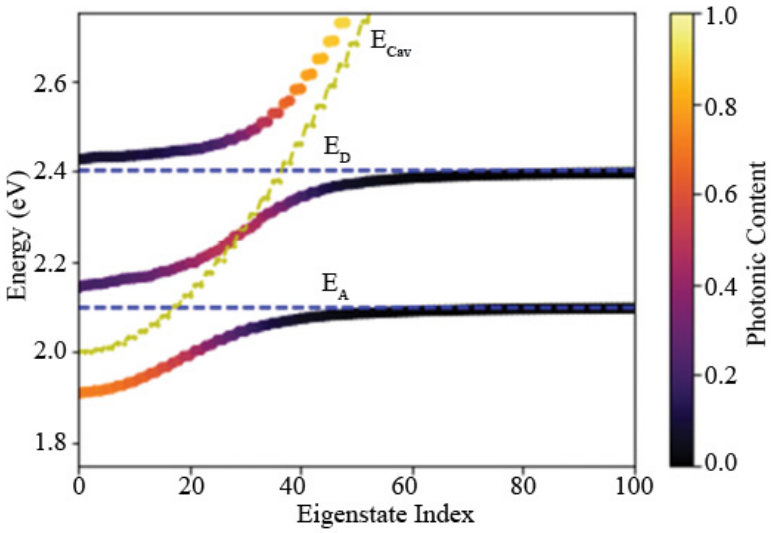

Figure 5. Dispersion plot of eigenstates derived from Hamiltonian of an ideal cavity system. The blue lines represent the excitation energies of the donor and acceptor molecules, and the yellow line represents the photonic energies. The photonic contents of the eigenstates are colored according to the legend on the right.

As shown in Figure 5, there are three bands that the eigenstates belong to. This contrasts with Figure 3, where there were only the UP and LP bands. The middle band that has energies between the donor and acceptor excitation energies can be denoted as the Middle Polariton, or MP. The MP arises when there are two different molecules that are strongly coupled with the cavity photons.

Using equation 4, the probability that an excited donor molecule will transition to the acceptor molecule after a near-infinite time has passed was calculated to be approximately $5.492x10^{-5}$. This transition probability is notably small; however, it must be noted that the transition probability would be much smaller if the cavity were to be removed. This is because of the large excitation energy gap between the donor and acceptor molecules and the large distances between neighboring molecules within the system. Furthermore, in this study's model, the donor and acceptor molecule are non-interacting, as shown by the lack of off-diagonal elements between the molecules in Equation 2. Thus, if the cavity were to be removed, the transition probability would be zero.

The ideal model thereby serves as a control to which future coherent calculations can be compared to. The fact that some transition probability is noted in the ideal model supports the idea that the cavity is crucial to mediating intermolecular energy transfer. However, further investigation can be conducted to determine which parameters can maximize the efficiency of intermolecular energy transfer.

3.2. Energetic Disorder Effects

One of these parameters that potentially improves the efficiency of coherent energy transfer within the cavity is the disorder in excitation energy for both the donor and acceptor molecules. In the ideal model, all donor molecules had excitation energies of 2.4 eV and all

acceptor molecules had excitation energies of 2.1 eV. This assumption does not fall in line with experimental measurements, since not all molecules will have the same ground state and excited state energies.

A Gaussian distribution with a specified standard deviation was incorporated into the model to determine the excitation energies for each molecule in the system. Transition probabilities were then calculated for each model generated. Figure 6 shows the change in transition probability as the disorder is increased.

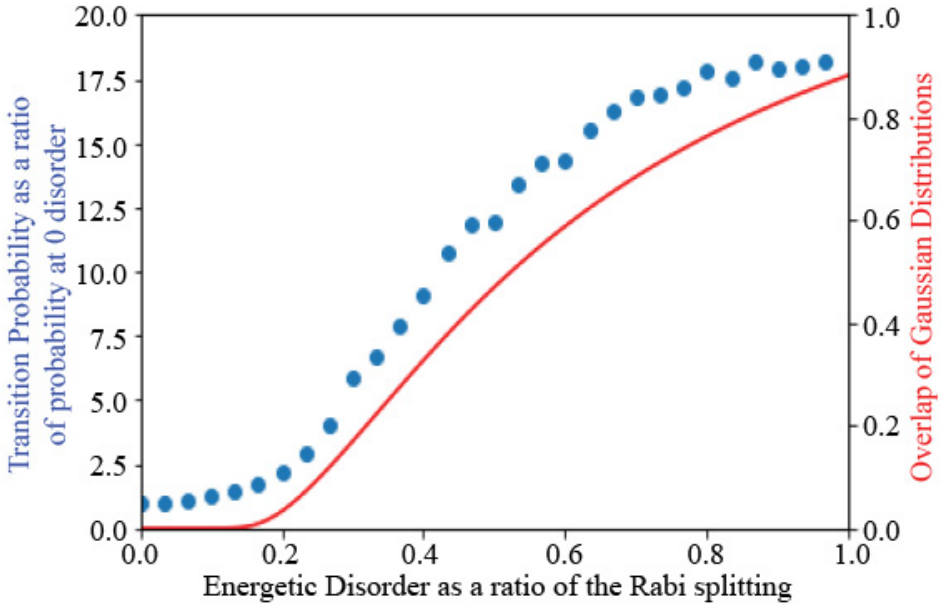

Figure 6. Change in donor to acceptor energy transition probability as a function of energetic disorder shown in blue. The energetic disorder is shown as a ratio of the Rabi splitting and the transition probability is shown as a ratio of the transition probability in the ideal system. The Rabi splitting was set at 0.3 eV and the transition probability at 0 disorder was calculated to be approximately $5.492x10^{-5}$. Absolute and relative transition probabilities at each energetic disorder are shown in Table S1. Each point was calculated as an average of 2,500 transition probabilities that came from 10 different realizations of the Hamiltonian. Overlap of Gaussian distributions between donor and acceptor molecules is shown in red.

As shown in Figure 6, the transition probability increases in a sigmoidal manner as the energetic disorder is increased. Furthermore, when the energetic disorder is increased to equal the value of the Rabi splitting, the transition probability increases by a factor of 18. This supports the idea that adding energetic disorder increases the efficiency of intermolecular energy transfer in the coherent case.

3.3. Comparison to Coulomb Model

Figure 6 also shows the overlap between the donor and acceptor Gaussian distributions. This overlap seems to follow the same trend as the transition probability trend. This raises the question whether the increase in transition probability is due to an increase in efficiency of intermolecular energy transfer via the cavity or due to the increased overlap in excitation energies due to the Gaussian distribution.

In answering this question, a comparison can be made between the case inside the cavity and the case outside the cavity. A model can be generated where the two types of molecules outside the cavity can transfer energy via a Coulomb interaction. The magnitude of Coulomb interaction needed to reach the same transition probability as inside the cavity can be calculated at different energetic disorder values.

Equation 10 shows the Hamiltonian of such a Coulomb interaction model. The magnitude of the Coulomb interaction is represented by J.

$$H = \begin{pmatrix} E_D & J & 0 & 0 \\ J & E_D & J & 0 \\ 0 & J & E_A & J \\ 0 & 0 & J & E_A \end{pmatrix}$$

Equation 10

As shown in equation 10, only molecules that are neighbors to each other in free space can interact via the Coulomb interaction. This "Nearest Neighbor" Hamiltonian can then be diagonalized, and transition probabilities can be calculated and compared to the cavity Hamiltonian.

Table 1 shows the magnitude of J necessary at different energetic disorder values to match the transition probability within a cavity.

Table 1. Magnitude of J in "Nearest Neighbor" Hamiltonian that is needed to generate a transition probability that matches the transition probability in the cavity Hamiltonian. Rabi splitting is set at 0.3 eV.

Energetic Disorder as a ratio of Rabi Splitting	J (eV)
0.0	0.04
0.1	0.04
0.5	0.09
1.0	0.16

As shown in Table 1, the Coulomb interaction needed for the "Nearest Neighbor" transition probability to match that of the cavity transition probability is unrealistically high. Even at the lowest J value, the dipole moment calculated using Coulomb's law would be 2979.96 D, a dipole moment that is 2 orders of magnitude larger than typical dipole moments [47]. This supports the idea that the overlap in Gaussian distributions of the energies between the two molecules is not the only factor causing the increase in transition probability within the cavity.

3.4. Distance Dependence

Previous research has shown how energy transfer within the cavity still occurs efficiently even when the donor and acceptor molecule are separated by large distances [22]. This distance independent relationship is what separates energy transfer dynamics within a cavity to the dynamics shown by FRET. This study's coherent calculations can support this distance independent relationship by generating Hamiltonians with different intermolecular distances and investigating the effects on transition probability.

Figure 7 shows the change in transition probability as energetic disorder changes for three different values of intermolecular distance "a".

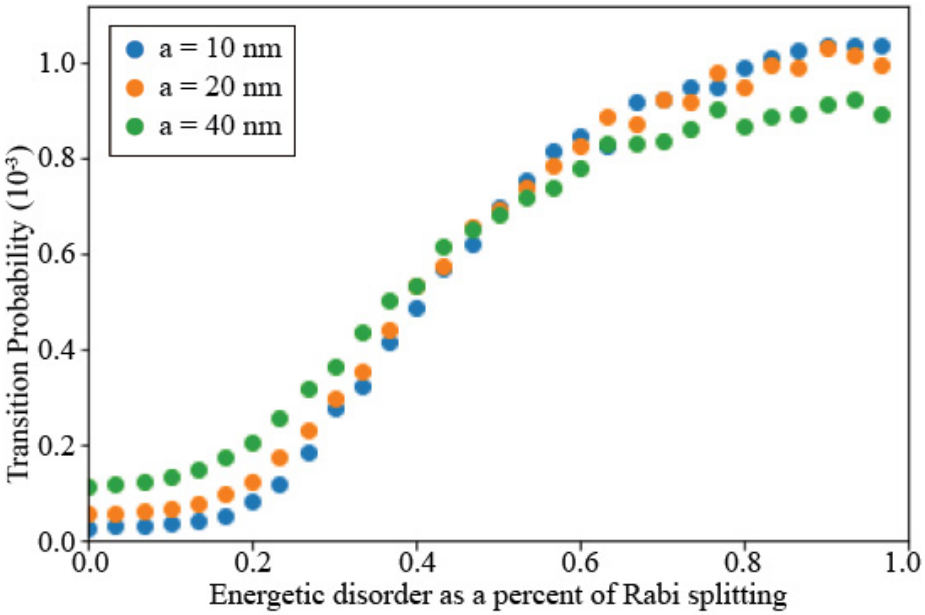

Figure 7. Absolute transition probability as a function of energetic disorder for different values of intermolecular distance. Rabi splitting is set at 0.3 eV. Each point was calculated as an average of 2,500 transition probabilities that came from 10 different realizations of the Hamiltonian. Figure 7 is reproduced with standard deviations in Figure S2. Absolute transition probabilities at the ideal case are $2.696x10^{-5}$, $5.489x10^{-5}$, and $1.129x10^{-4}$ for intermolecular distances of 10 nm, 20 nm, and 40 nm respectively. Absolute transition probabilities at the case

with highest energetic disorder are $1.034x10^{-3}$, $9.912x10^{-4}$, and $8.915x10^{-4}$ for intermolecular distances of 10 nm, 20 nm, and 40 nm respectively.

As shown in Figure 7, the transition probabilities at each energetic disorder value are relatively similar and follow the same trend as energetic disorder increases. The standard deviations for each point (shown in Figure S2) overlap for all points past an energetic disorder of 0.1 times the Rabi splitting. This supports the idea that intermolecular energy transfer is distance independent inside the cavity.

Another trend can be seen from Figure 7. The transition probability at low energetic disorder is higher for larger intermolecular distances, but the transition probability at high energetic disorder switches to being lower for larger intermolecular distances. Even though the standard deviations overlap generously, the averages still show this interesting trend. This trend is not solely due to fluctuations in incorporating disorder into the system, since the trend is still seen with a greater number of trials incorporated.

In pursuit of an explanation for the trend, the molecular content within the MP was investigated for different energetic disorders at different intermolecular distances. The MP is thought to be an important intermediate in facilitating energy transfer between donor and acceptor molecules within the cavity [11], thus it could provide insight to the trend seen in Figure 7. Figure 8 shows the total molecular content within the MP states as a function of energetic disorder at different intermolecular distances. The MP states were designated as the middle third eigenstates from the Hamiltonian. The total molecular content was calculated by summing the product of the probability of an eigenstate to be a donor molecule and the probability of an eigenstate to be an acceptor molecule over all MP eigenstates.

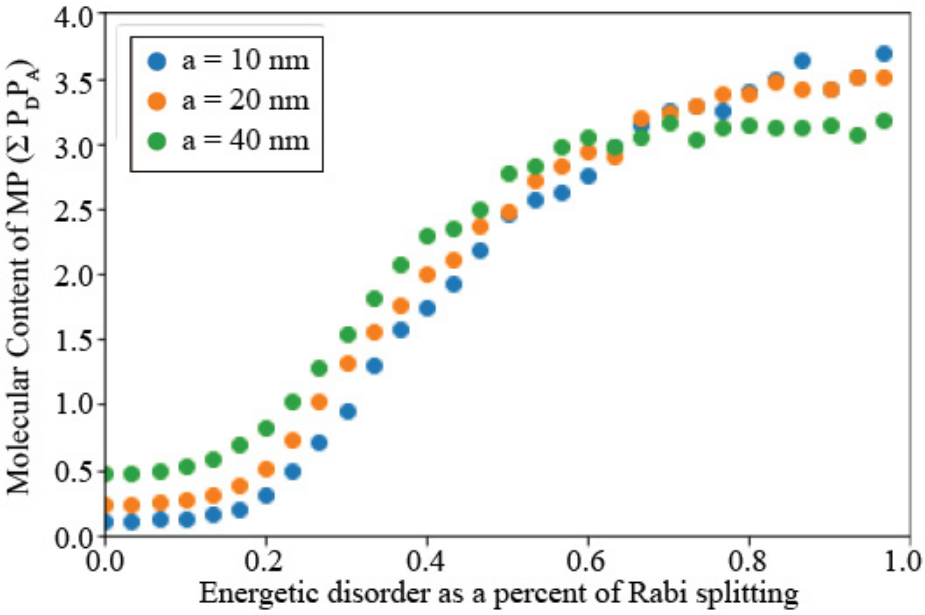

Figure 8. Change in molecular content (summation of donor and acceptor content over all MP states) within the MP as a function of energetic disorder for different intermolecular distances. Rabi splitting was set at 0.3 eV. Each trend was calculated by averaging MP molecular contents from 10 different realizations of the Hamiltonian.

As shown in Figure 8, the molecular content within the MP seems to follow the same trends at different intermolecular distances as in Figure 7. This would explain the trend seen in Figure 7, however the reasons why the molecular content changes in such a way are still unknown.

It is possible to explain the initial difference between the three curves in Figure 7. In the figure, the calculations with further intermolecular distances had greater transition probability at smaller energetic disorders. This could be due to the change in molecular dipole moment as the density of molecules within the cavity decreases. The Rabi splitting is proportional to the single molecule molecular dipole moment multiplied by the square root of the density within the cavity. Thus, if the Rabi splitting stays constant, the single molecule molecular dipole moment would need to increase if the density decreased. This would strengthen the interaction between each

molecule and the cavity and aid in the transfer of energy from donor to acceptor molecules. However, this explanation falls apart at higher energetic disorders, since Figure 7 shows the transition probabilities being flipped at the end of the trend.

3.5. Relevance of Cavity Detuning

The dependence of the transition probability on the energy distribution of the cavity was also investigated. In most calculations, the lowest energy cavity photon was set at 2.0 eV, lower than both the donor and acceptor molecular transition energies. This would allow the span of cavity photons to interact with both the donor and acceptor molecules. Raising or lowering the energy of the lowest energy cavity photon could potentially affect the number of polaritonic states generated in the cavity.

Figure 9 shows the effects of the energy of the cavity on transition probability. The cavity was detuned by changing the energy of the lowest energy cavity photon.

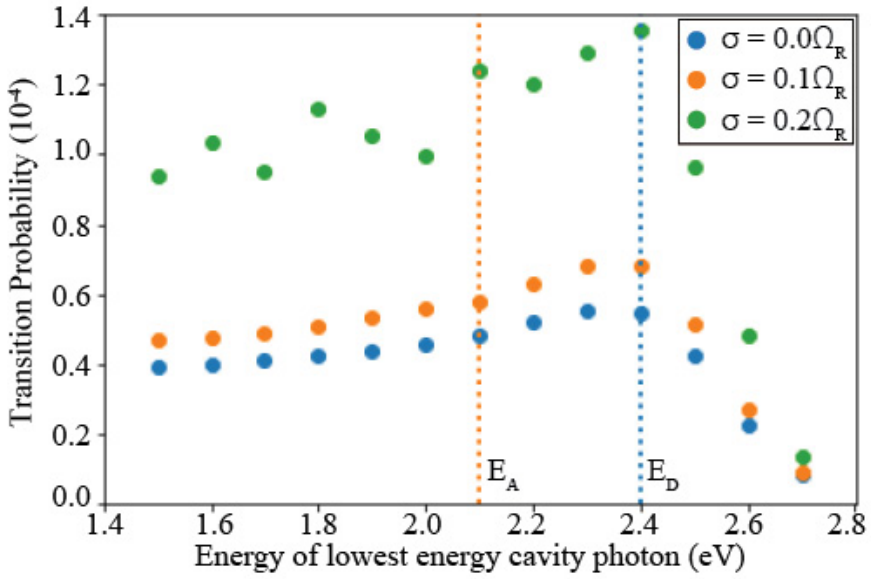

Figure 9. Absolute transition probability as a function of the energy of the lowest energy cavity photon at different energetic disorder (σ). Rabi splitting (Ω_R) is set at 0.3 eV. Each point was

calculated as an average of 2,500 transition probabilities that came from 10 different realizations of the Hamiltonian.

As seen in Figure 9, the transition probability decreases once the cavity becomes too high energy to reliably interact with both the donor and acceptor molecules. However, there does seem to be a maximum of transition probability when the lowest energy cavity photon has an energy in between the transition energies of the donor and acceptor molecules. This maximum may be due to the maximization in the number of cavity photons which are simultaneously near-resonant with both the donor and acceptor molecules.

4. Open Quantum System Dynamics

Open quantum system dynamics use the Hamiltonian generated previously to look at the evolution of the system as a function of time. Unlike the infinite-time dynamics in the previous section, open system dynamics look at smaller time scales to gain insight into the mechanism in which the energy is being transferred.

4.1. Classification of Eigenstates

The open quantum system dynamic calculations also aim to investigate the effects of disorder on the rates of energy transfer between donor and acceptor molecules. However, unlike the coherent energy transfer calculations, where categorization of eigenstates follows the schematic shown in Figure 2a, the open quantum system energy transfer calculations take dark states into account – eigenstates that are weakly coupled to the cavity. Thus, a new classification scheme is needed to separate dark states from polaritonic states.

The model incorporated this new classification scheme by considering photonic content within each state. Figure 10 shows the photonic and molecular probabilities within each eigenstate from a Hamiltonian with zero energetic disorder.

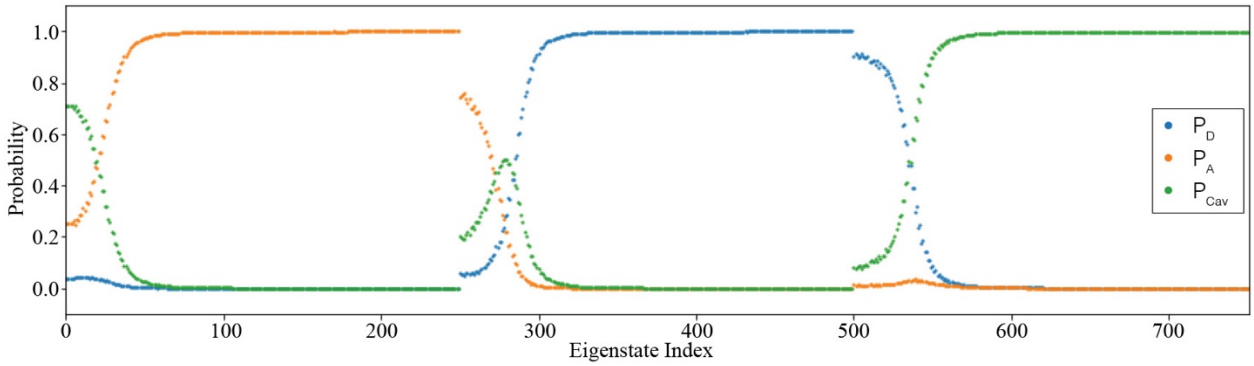

Figure 10. Probability of an eigenstate to be a cavity photon, a donor molecule, or an acceptor molecule in an ideal system.

Based on the classification scheme used for the closed system calculations, the first 250 eigenstates would be considered LP, the second 250 would be MP, and the last 250 would be UP. For the open quantum system calculations, any state with lower than 0.1 probability of being a cavity photon would be considered a dark state (either a dark donor or a dark acceptor depending on its energy). Additionally, any state with greater than 0.9 probability of being a cavity photon would be considered a photonic state and would be disregarded from the calculations.

It can be seen from Figure 10 that there would potentially be a greater number of dark states than polaritonic states. This observation is confirmed by the code classifying approximately 35% of the states as dark donor states and approximately 35% of states as dark acceptor, forcing the three different polaritonic states to share the last 30% of states between each other. Because the number of dark states is greater than number of polaritonic states, there would be an inherent bias for the energy to move to the dark states. Additionally, with the molecular thermal relaxation rate being four orders of magnitude smaller than the photonic relaxation rate, the bias becomes even greater in favor of the dark states. This aids in transferring energy to the dark states from the polaritonic states.

We apply the classification scheme described above only to samples with small energetic disorder, as ambiguity arises when the excited-state energy fluctuations are sufficiently large. Figure 11 shows the probabilities of each eigenstate when the energetic disorder was increased to equal the Rabi splitting at 0.3 eV.

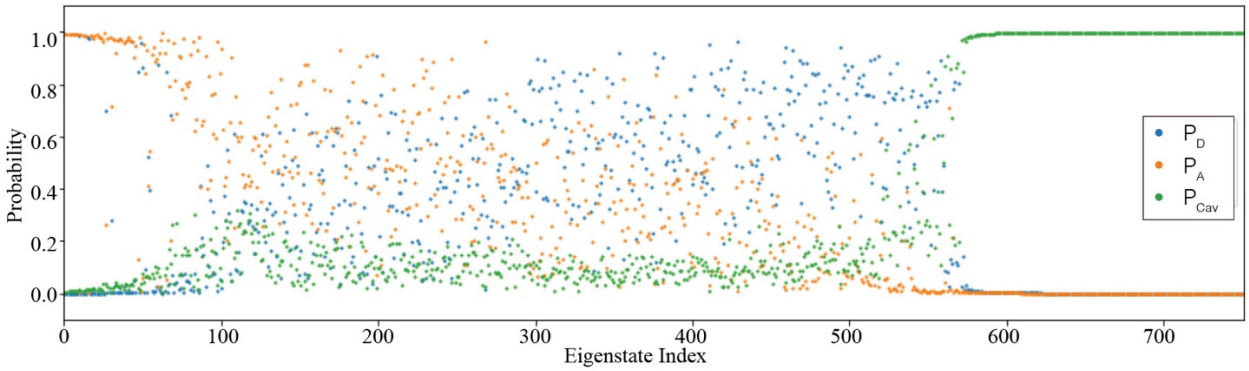

Figure 11. Probability of an eigenstate to be a cavity photon, a donor molecule, or an acceptor molecule with energetic disorder equal to Rabi splitting (0.3 eV).

As seen in Figure 11, the higher energetic disorder led to a chaotic energy distribution for polaritonic and dark states that imposed challenges to the classification scheme. However, this scheme was functional at weak energetic disorder below 10% of the Rabi splitting, thus only those cases were explored in the open quantum system dynamic calculations.

4.2. Time Evolution of Energy Transfer

Once all eigenstates were classified into one of five states (LP, dark acceptor, MP, dark donor, UP), the evolution of energy transfer could be investigated. A range of eigenstates within a specified energy window in the UP were excited, and the probability of an excitation to be found within each state was plotted as a function of time to gain insight into the time dynamics of the system. Figure 12a shows the evolution of an ideal system as a function of time.

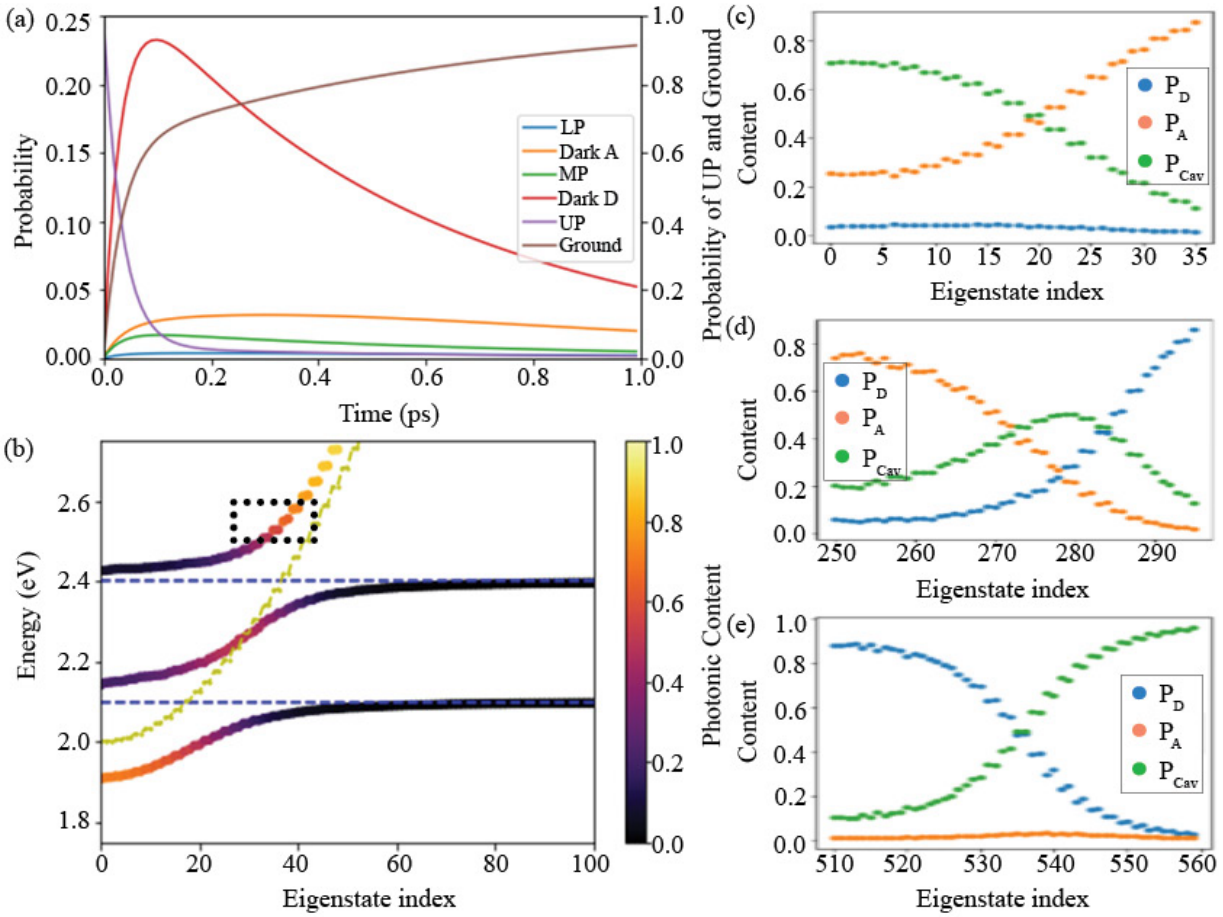

Figure 12. Kinetic observables of an ideal system (disorder is 0, intermolecular distance is 20nm). Calculations were done using one realization of the Hamiltonian. (a) Time dependent evolution of probabilities within each state. Dark D represents dark donor and Dark A represents dark acceptor. Ground represents the probability that the excitation has decayed via photonic leakage through the cavity or via thermal relaxation through the molecules. (b) Dispersion plot of system. Dotted black rectangular box represents states that were excited. Excitation window was kept between 2.51 and 2.61 eV. (c) (d) (e) Photonic and molecular content of each eigenstate within LP, MP, and UP respectively.

As shown in Figure 12a, the energy begins in the UP (purple line) and gets transferred within a short amount of time to dark donor (red line). Some probability from the excitations

within UP can be seen in dark acceptor and MP (orange and green line respectively) only after a short timescale of approximately 0.1ps.

The ground line represents the rate at which the excitation decays from the cavity. With the excitation beginning in the UP, if no energy transfer occurs, then the system should decay to 1/e within approximately 0.06 picoseconds. However, it seems as if the system takes over 0.1 picoseconds to do so, supporting the idea that the energy has transferred over to the dark states, since the molecular decay rate is much slower. Thus, the time evolution of this cavity model supports an intermolecular transfer mechanism that is faster than the decay rate of the photons within the system.

The same graphs were produced for models with energetic disorder incorporated into them. Models with energetic disorder of 0.015 eV and 0.03 eV (0.05 and 0.1 times the Rabi splitting of 0.3 eV respectively) were generated and their kinetics are shown in Figures S4 and S5 (Figure 12 is duplicated on Figure S3 for comparison). Figure 13 compares the “Ground” line for each of these three energetic disorder cases, along with a case where the energetic disorder is equal to the Rabi splitting of 0.3 eV.

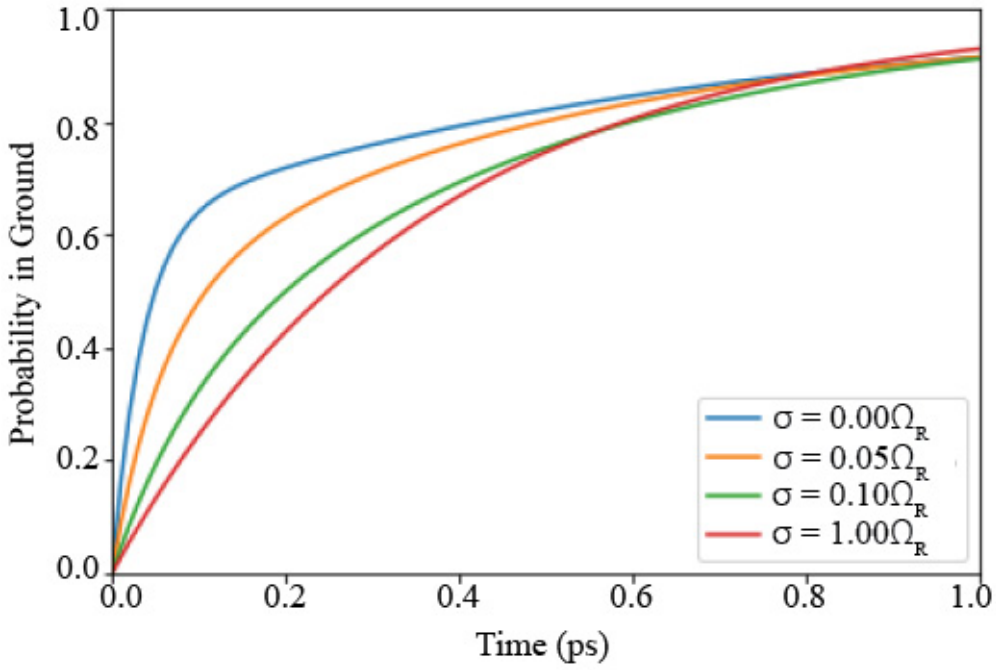

Figure 13. Probability that excitation within cavity has leaked (Ground) at different energetic disorder (σ) values. Rabi splitting (Ω_R) is set at 0.3 eV.

As shown in Figure 13, the rate at which the excitation leaks from the cavity seems to be slower at higher energetic disorder values before converging at higher time scales. Additionally, the slower leakage rate saturates at higher energetic disorder values, as shown by the case when energetic disorder is equal to the Rabi splitting. However, when comparing Figure 12a with Figures S4a and S5a, the probability of the dark donor or dark acceptor does not increase as energetic disorder increases. In fact, the probability of both dark donor and dark acceptor seems to decrease as energetic disorder increases at time 0.6 ps. Thus, the slower decay rate shown in Figure 13 does not definitively show the increased energy transfer with greater energetic disorder in the open quantum system case. The trend could be due to the greater localization in dark states at higher disorder values, causing some states to have a much higher molecular content than expected.

4.3. Energy Transfer Efficiency

One way to quantitatively compare the efficiency of energy transfer for different energetic disorder cases would be to investigate the ratio of the probability in the dark donor state to the probability in the dark acceptor state at a time when the system is in a quasi-equilibrium state. A UP state that is excited at the beginning of each calculation has a specific donor molecular content and acceptor molecular content and therefore has a specific donor to acceptor ratio. If energy were to be transferred from the UP state directly to the dark donor or dark acceptor state, the donor to acceptor ratio of the initial excited state would equal the ratio of the probability in the dark donor state to the probability in the dark acceptor state at quasi-equilibrium. However, if the initial ratio is larger than the ratio at quasi-equilibrium, substantial energy transfer would have occurred through other means (a similar comparison was made in the experiments reported at Ref [18]).

Figure 14 shows the comparison of the initial donor to acceptor ratio (P_D/P_A) compared to the equilibrium donor to acceptor ratio with zero energetic disorder. A quasi-equilibrium was established as the time at which both the first and second derivatives of the dark donor curve were small enough after the dark acceptor curve had hit its maximum in the time evolution graph.

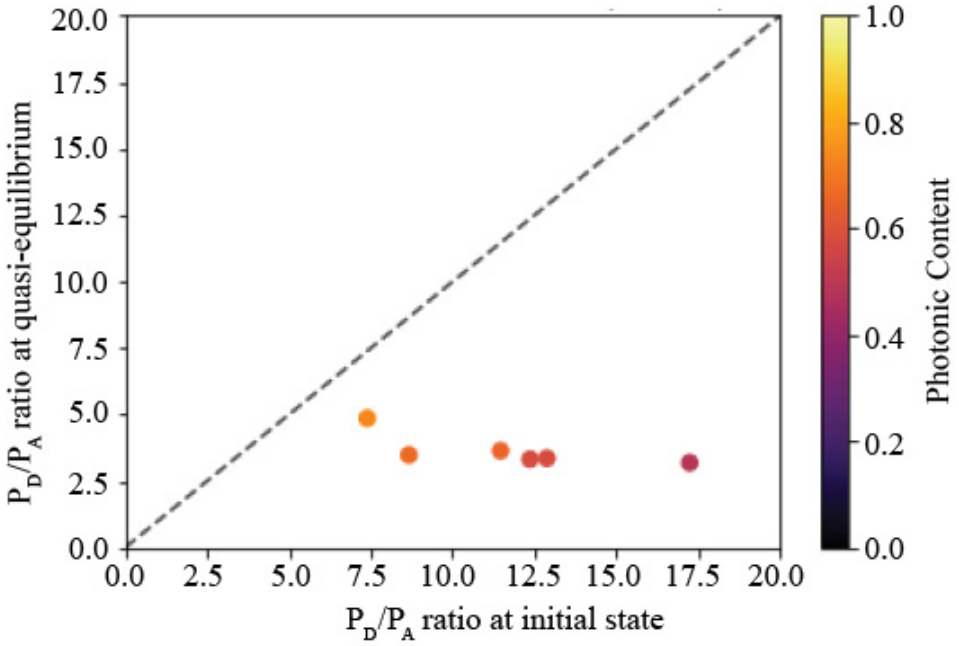

Figure 14. Comparison of P_D/P_A ratio at the initial excited state and the P_D/P_A ratio at quasi-equilibrium for the ideal model. Each point represents one state within the energetic window shown in Figure 12b that was excited. Only one realization of the Hamiltonian was used. Diagonal line is for reference. Exact P_D/P_A ratios for all points on graph are shown in Table S2.

As shown in Figure 14, all points are under the diagonal line, supporting the notion that there was more than just direct energy transfer from the UP to both dark donor and dark acceptor molecules. Data points shown in Table S2 are also comparable to experimental data collected by Ref [18].

This P_D/P_A ratio comparison can be extended to models with energetic disorder. Figure 15 shows the P_D/P_A ratio comparisons for three different energetic disorder cases.

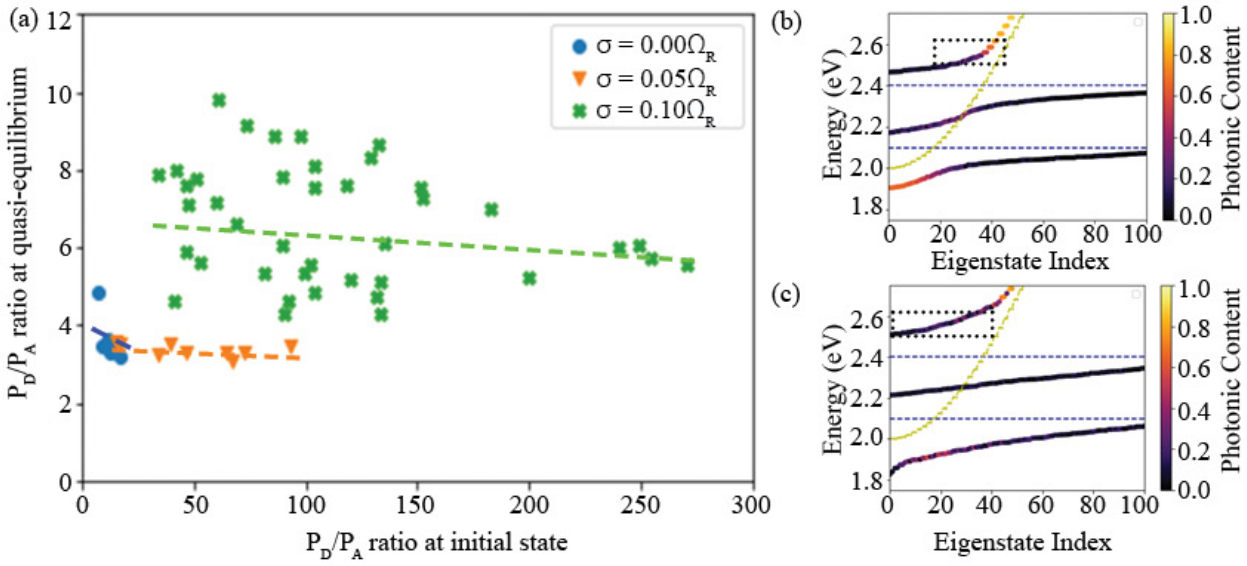

Figure 15. (a) P_D/P_A ratio at initial excited state and P_D/P_A ratio at quasi-equilibrium for three different energetic disorder (σ) values. Trend lines for each energetic disorder value are shown. Rabi splitting (Ω_R) is set at 0.3 eV. Diagonal line is removed since plot is disproportionally zoomed in to enhance figure visibility. Full figure with diagonal line is shown in Figure S9. Figure S7 and S8 show the P_D/P_A ratio comparisons for models with 0.05 Ω_R and 0.10 Ω_R energetic disorder respectively. All points are generated using one realization of the Hamiltonian. (b) (c) Dispersion plots for systems with 0.05 Ω_R and 0.10 Ω_R energetic disorder respectively. The black box shows the states excited within the window of 2.51 and 2.61 eV. A greater number of states are included within the excitation energetic window as the energetic disorder increases.

As shown in Figure 15, the P_D/P_A ratios undergo a much greater decrease relative to the initial state when the energetic disorder of the system is increased. This observation supports the idea that greater indirect energy transfer is occurring in the cases where energetic disorder is incorporated into the model. Furthermore, the P_D/P_A ratios at quasi-equilibrium for each energetic disorder case seem to converge at a specific P_D/P_A ratio (as shown by the trendline

nearing a horizontal line). Thus, the system seems to have a lack of memory of the initial state, since the initial P_D/P_A ratios are much broader than the P_D/P_A ratios at quasi-equilibrium.

It can be noted that there is a greater spread in the P_D/P_A ratio at equilibrium for the case where energetic disorder is 10% of the Rabi splitting. Thus, there could be more memory in the higher energetic disorder cases. However, because the calculations were done with only one realization of the Hamiltonian, this observation could be solely due to the fluctuations in disorder. More realizations of the Hamiltonian and an averaging procedure would be needed to probe in more detail for whether the P_D/P_A distribution at quasi-equilibrium shows significant memory effects which become more relevant with increasing energetic disorder.

This convergence of the P_D/P_A ratio does not seem to converge to an expected equilibrium. The P_D/P_A ratio at equilibrium converges to a ratio above 1. This would suggest a bias towards the dark donor molecules. Because the system was set with no thermal bias, total equilibrium would consist of a P_D/P_A ratio of approximately 1 at equilibrium. This is not seen in Figure 15. This could potentially be because the UP was excited in this case. If the LP was excited, the P_D/P_A ratio at equilibrium would likely be lower than 1. This lack of thermalization and initial state dependence is a byproduct of the transient and leaky nature of the excited-state dynamics. In the absence of cavity leakage, in fact, we observe an equilibrium constant of approximately one.

4.4. Intraband Dynamics

Investigating the dynamics within a specific category of states, or band, could be key to gain insight into the dynamics governing the transfer of energy between donor and acceptor molecules within the open quantum system calculations. Thus, a category could be broken up into five different energetic groups, and time evolution plots can be generated to show the

probability within those five groups. Figure 16 compares the intra-band dynamics for the MP band at different energetic disorder values.

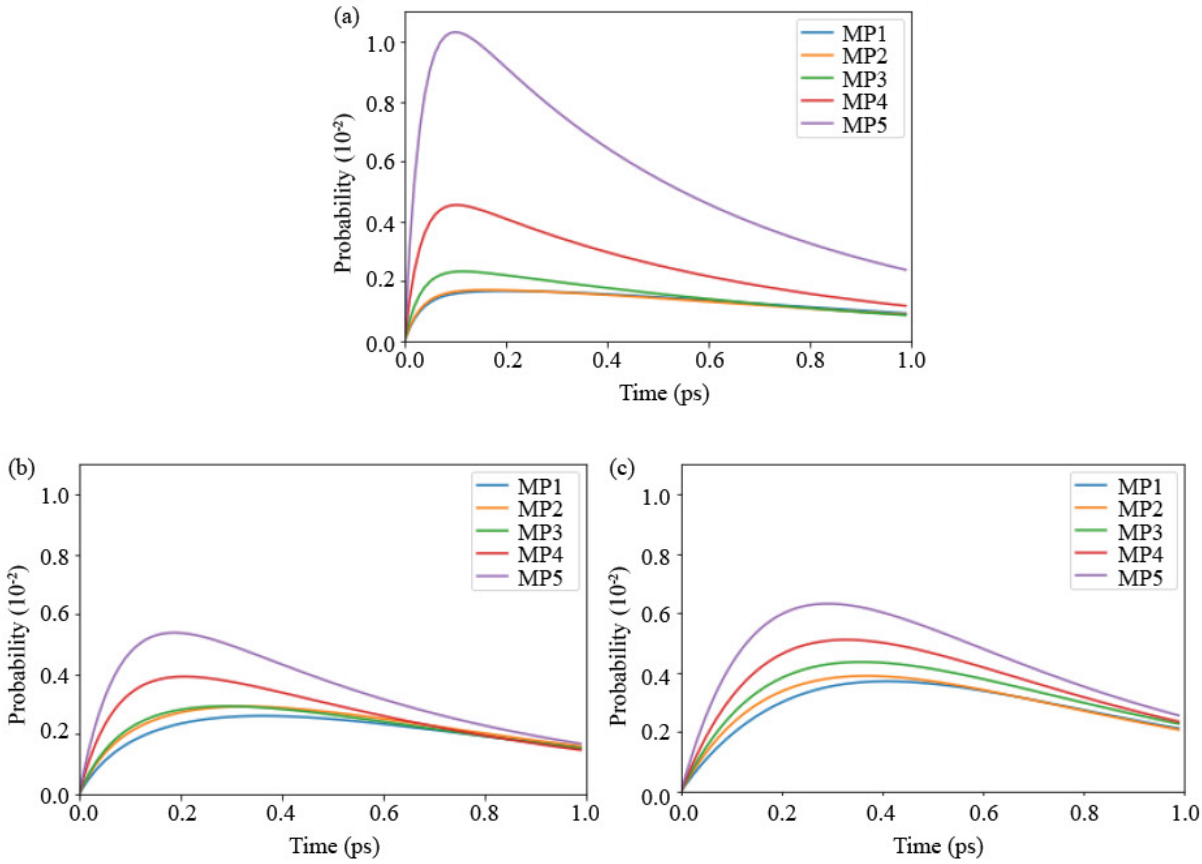

Figure 16. MP intra-band time evolution dynamics for models with (a) 0 eV, (b) 0.015 eV, (c) and 0.03 eV energetic disorder — 0, 0.05, and 0.1 times the Rabi splitting of 0.3 eV respectively. The MP band was divided into five categories with MP1 being the lowest energy category and MP5 being the highest energy category. Each category had the same number of MP states.

As shown in Figure 16, all portions of the MP band become excited all at once before transferring energy to other bands in the system. This mechanism is different from the mechanism that the energy transfers to the higher energy band first, since it is closest in energy to the UP or the dark donor, before trickling down the energetic sections within the MP to eventually being transferred to the dark acceptor once arriving at the lowest energy portion of the

band. Instead, the energy is transferred to all portions of the MP, with the higher energy portions receiving greater preference due to its proximity in energy to the UP or the dark donor.

There is another trend in Figure 16. As energetic disorder increases, the lowest energy portion of the MP band increases in maximum probability. This could be a potential explanation for the trend in Figure 15. With the lower energy portion of the MP band having a higher probability, more energy can be transferred efficiently to the dark acceptor molecules, since the lower energy portions are the polaritons closer in energy to the dark acceptor molecules. Thus, there would be more efficient energy transfer in the higher energetic disorder cases due to the trend in Figure 16.

4.5. Coarse Grained Approach

All calculations analyzed in sections 4.2, 4.3, and 4.4 used the method described in section 2.2, where rate kinetics were calculated for the transfer of energy from each eigenstate to the next (referred to as full matrix calculations). With only 751 eigenstates, the computational cost was not too high (calculations took approximately five minutes for each model generated). However, if models with a greater number of eigenstates were to be created, the computational cost could potentially become overwhelming. Thus, a coarse-grained matrix can be generated to average the kinetics of the states within each category before diagonalization to minimize computational cost.

The coarse-grained matrix is a 5 by 5 matrix that contains kinetic rates for the transition from one category to the next. Thus, all eigenstates that were categorized to be an LP state had the same kinetic dynamics. Even in this study where the Hamiltonian generated contained a relatively small number of eigenstates (751), the computations using the coarse-grained matrix decreased the computational time to approximately 5 seconds.

The coarse-grained calculations were consistently similar to the full matrix calculations when considering the time evolution dynamics of the system. Figure 17 compares the time evolution dynamics from the coarse-grained matrix to the full matrix calculations for an ideal model.

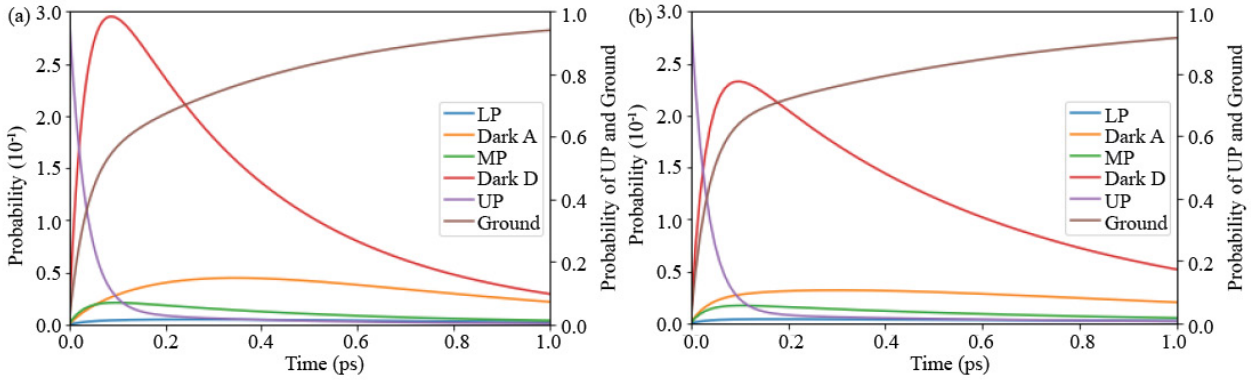

Figure 17. Time evolution of probabilities of each state using (a) coarse-grained and (b) full matrix calculations.

As shown in Figure 17, the coarse-grained calculations led to greater probabilities for most categories, causing the ground state to grow slower than the full matrix calculations. However, the dynamics were still similar. Thus, the trade-off between the computational cost of the full matrix calculations and the difference in results from the coarse-grained calculations can be weighed.

5. Conclusion and Future Directions

The purpose of this work was to investigate computational models representing polaritonic systems to determine optimal conditions for intermolecular energy transfer and understand time evolved dynamics governing the system.

The models generated allowed calculation of transition probabilities and time evolved dynamics. Using these calculations, experimental results concerning distance-independent energy transfer were supported, since transition probabilities were approximately the same at

different intermolecular distances. Furthermore, the calculations supported an indirect mechanism of energy transfer from the UP to the dark donor and acceptor states, shown by the change in P_D/P_A ratio from the initial state to the equilibrium state.

Regarding energetic disorder, section 3 showed how incorporating energetic disorder into the models can improve transition probabilities by factors of 18. These transition probabilities are much larger in comparison to transition probabilities outside a strong coupling regime. The importance of energetic disorder is also shown in section 4, where the time evolution dynamics were impacted. The change in P_D/P_A ratio from the initial state to the equilibrium state was much greater in the models with energetic disorder, supporting the notion that more energy transfer was facilitated by the cavity in cases with disorder. Energy decayed from the system at a slower rate initially in cases with energetic disorder, possibly allowing more energy transfer to occur before quasi-equilibrium is reached.

Future research would focus on expanding the models to further explain experimental results. 2-dimensional or 3-dimensional models could be applied, and the system dynamics could be compared. Future research would also focus on additional investigations of time evolved dynamics to provide insight into the mechanism in which energy is being transferred from donor to acceptor molecules. An averaging procedure could be added to see the dynamics after realizing multiple Hamiltonians at higher energetic disorder, providing insight into the average dynamics of the open quantum system. The combined effects of energetic disorder and thermal bias could also be studied as both can be relevant in experimentally studied organic exciton-polariton systems.

References

[1] Balzani, V.; Ceroni, P.; Juris, A. *Photochemistry and Photophysics; Concepts, Research, Applications*; John Wiley & Sons:Weinheim, 2014.

[2] Ebbesen, T. W. Hybrid Light-Matter States in a Molecular and Material Science Perspective. *Acc. Chem. Res.* **2016**, 49, 2403-2412.

[3] Agulló-López, F.; Cabrera, J. M.; Agulló-Rueda, F. Electrooptics: Phenomena, Materials and Applications. New York: Academic Press. 1994, 193-218.

[4] Thomas, A.; George, J.; Shalabney, A.; Dryzhakov, M.; Varma, S. J.; Moran, J.; Chervy, T.; Zhong, X.; Devaux, E.; Genet, C.; Hutchinson, J. A.; Ebbesen, T. W. Ground-state chemical reactivity under vibrational coupling to the vacuum electromagnetic field. *Angew. Chem. In. Ed.* **2016**, 55, 11462-11466.

[5] Thomas, A.; Lethuillier-Karl, I.; Nagarajan, K.; Verganwe, R. M. A.; George, J.; Chervy, T.; Shalabney, A.; Devaux, D.; Genet, C.; Moran, J.; Ebbesen, T. W. Tilting a ground-state reactivity landscape by vibrational strong coupling. *Science*, **2019**, 363, 615-619.

[6] Martínez-Martínez, L. A.; Du, M. Ribeiro, R. F.; Kéna-Cohen, S.; Yuen-Zhou, J. Polariton-assisted singlet fission in acene aggregates. *J. Phys. Chem. Lett.* **2018**, 9, 1951-1957.

[7] Kavokin, A. V.; Baumberg, J. J.; Malpuech, G.; Laussy, F. P. *Microcavities*; Oxford University Press, 2017; vol. 21.

[8] Austerlitz, H. Analog Signal Transducers. *Data Acquisition Techniques using PCs*, Academic Press, 2003; vol. 2, 6-28.

[9] Baranov, D. G.; Wersäll, M.; Cuadra, J.; Antosiewicz, T. J.; Shegai, T. Novel Nanostructures and Materials for Strong Light-Matter Interactions. *ACS Photonics*. **2018**, 5, 24-42.

[10] Ribeiro, R. F.; Martínez-Martínez, L. A.; Du, M.; Campos-Gonzalez-Angulo, J.; Yuen-Zhou, J.; Polariton chemistry: controlling molecular dynamics with optical cavities. *Chem. Sci.* **2018**, 9, 6325-6339.

[11] Coles, D. M.; Somaschi, N.; Michetti, P.; Clark, C.; Lagoudakis, P. G.; Savvidis, P. G.; Lidzey, D. G. Polariton-mediated energy transfer between organic dyes in a strongly coupled optical microcavity. *Nature Materials.* **2014**, 13, 712-719.

[12] Shalabney, A.; George, J.; Hutchison, J.; Pupillo, G.; Genet, C.; Ebbesen, T.W. Coherent coupling of molecular resonators with a microcavity mode. *Nature*. **2014**, 6, 5981

[13] Kimble, H. J. *Cavity Quantum Electrodynamics*; Academic Press: San Diego, 1994.

[14] Li, T. E.; Nitzan, A.; Subotnik, J. E. Collective Vibrational Strong Coupling Effects on Molecular Vibrational Relaxation and Energy Transfer: Numerical Insights via Cavity Molecular Dynamics Simulations. *Angew. Chem. Int. Ed.* **2021**, 60, 15533-15540.

[15] Schwartz, T.; Hutchinson, J. A.; Leanord, J.; Genet, C.; Haacke, S.; Ebbesen, T. W. Polariton dynamics under strong light-molecule coupling. *Chem. Phys. Chem.* **2013**, 14, 125-131.

[16] Jaynes, E. T.; Cummings, F. W. *Proc. IEEE*. **1963**, 51, 89-109.

[17] Tavis, M.; Cummings, F. W. Exact Solution for an N-Molecule —Radiation-Field Hamiltonian. *Phys. Rev.* **1968**, 170, 370-384.

[18] Tavis, M.; Cummings, F. W. Approximate Solution for an N-Molecule—Radiation-Field Hamiltonian. *Phys. Rev.* **1969**, 188, 692-695.

[19] Houndré, R.; Stanley, R. P.; Ilgems, M. Vacuum-Field Rabi Splitting in the Presence of Inhomogeneous Broadening: Resolution of a Homogeneous Linewidth in an

Inhomogeneously Broadened System. *Phys. Rev. A: At./ Mol./ Opt. Phys.* **1996**, 53, 2711-2715.

[20] Rabi, I. I. Space Quantization in a Gyrating Magnetic Field. *Phys. Rev.* **1937**, 51, 652-654.

[21] Agarwal, G. S. Vacuum-Field Rabi Splittings in Microwave Absorption by Rydberg Atoms in a Cavity. *Phys. Rev. Lett.* **1984**, 53, 1732-1734.

[22] Zhong, X.; Chervy, T.; Zhang, L.; Thomas, A.; George, J.; Genet, C.; Hutchinson, J. A.; Ebbesen, T. Energy transfer between spatially separated entangled molecules. *Angew. Chem. Int. Ed.* **2017**, 56, 9034-9038.

[23] Förster, T. Zwischenmolekulare Energiewanderung und Fluoreszenz. *Ann. Phys.* **1948**, 437, 55-75.

[24] Scholes, G. D. Long Range Resonance Energy Transfer in Molecular Systems. *Annu. Rev. Phys. Chem.* **2003**, 54, 57-87.

[25] Mendintz, I. L.; Hildebrandt, N. FRET – Förster Resonance Energy Transfer: From Theory to Applications. John Wiley & Sons. 2013.

[26] Georgiou, K.; Jayaprakash, R.; Othonos, A.; Lidzey, D. G. Ultralong-Range Polariton Assisted Energy Transfer in Organic Microcavities. *Angew. Chem. Int. Ed.* **2021**, 60, 16661-16667.

[27] Du, M.; Martínez-Martínez, L. A.; Ribeiro, R. F.; Hu, Z.; Menon, V. M.; Yuen-Zhou, J. Theory for polariton-assisted remote energy transfer. *Chem. Sci.* **2018**, 9, 6659-6669.

[28] Xiang, B.; Ribeiro, R. F.; Dunkelberger, A. D.; Wang, J.; Li, Y.; Simpkins, B. S.; Owrutsky, J. C.; Yuen-Zhou, J.; Xiong, W. Two-dimensional infrared spectroscopy of vibrational polaritons. *PNAS*. **2018**, 115(19), 4845-4850.

[29] Dunkelberger, A. D.; Spann, B. T.; Fears, K. P.; Simpkins, B. S.; Owrutsky, J. C. Modified relaxation dynamics and coherent energy exchange in coupled vibration-cavity polaritons. *Nat. Commun.* **2016**, 7, 13504.

[30] Xiang, B.; Ribeiro, R. F.; Du, M.; Chen, L.; Yang, Z.; Wang, J.; Yuen-Zhou, J.; Xiong, W. Intermolecular vibrational energy transfer enabled by microcavity strong light-matter coupling. *Science.* **2020**, 368, 665-667.

[31] Ribeori, R. F. Strong Light-Matter Effects on Molecular Ensembles. *Chem. Phys.* **2021**. https://arxiv.org/abs/2107.07032.

[32] Kuther, A.; Bayer, M.; Gutbrod, T.; Forchel, A.; Knipp, P. A.; Reinecke, T. L.; Werner, R. Confined optical modes in photonic wires. *Phys. Rev. B.* **1998**, 58(23), 15744-15748

[33] Zhang, S.; Shang, Q.; Du, W.; Shi, J.; Wu, Z.; Mi, Y.; Chen, J.; Liu, F.; Li, Y.; Liu, M.; Zhang, Q.; Liu, X. Strong Exciton-Photon Coupling in Hybrid Inorganic-Organic Perovskite Micro/Nanowires. *Adv. Opt. Mat.* **2017**, 6(2), 1701032.

[34] Savona, V.; Andreani, L. C.; Schwendimann, P.; Quattropani, A. Quantum well excitons in semiconductor microcavities: Unified treatment of weak and strong coupling regimes. *Solid State Commun.* **1995**, 93, 733-739.

[35] Petruccione, F.; Breuer, H. P. The Theory of Open Quantum Systems. United Kingdom: Oxford University Press. 2002.

[36] Zwanzig, R. Nonequilibrium Statistical Mechanics. New York: Oxford University Press. 2001.

[37] Michetti, P.; La Rocca, G. C. Simulation of J-aggregate microcavity photoluminescence. *Phys. Rev. B.* **2008**, 77, 195301.

[38] Dirac, P. A. M. The quantum theory of the emission and absorption of radiation. *Proc. R. Soc. London, Ser. A.* **1927**, 114, 243-256.

[39] del Pino, J.; Feist, J.; Garcia-Vidal, F. J. Quantum theory of collective strong coupling of molecular vibrations with a microcavity mode. *New J. Phys.* **2015**, 17.

[40] Martínez-Martínez, L. A.; Yuen-Zhou, J. Comment on 'Quantum theory of collective strong coupling of molecular vibrations with a microcavity mode.' *New J. Phys.* **2018**, 20.

[41] Kuriyan, J.; Konforti, B.; Wemmer, D. The Molecules of Life: Physical and Chemical Principles. New York: Garland Science: Taylor and Francis Group. 2013.

[42] Litinskaya, M. R. P. A. V. M. Fast polariton relaxation in strong coupled organic microcavities. *J. Lumin.* **2004**, 110, 364-372.

[43] Piskunov, N. Differential and Integral Calculus. Moscow: MIR Publishers. 1969.

[44] Van Kampen, N. Stochastic Processes in Physics and Chemistry. Netherlands: Elsevier Science. 1992.

[45] Pscherer, A.; Meierhofer, M.; Wang, D.; Kelkar, H.; Martín-Cano, D.; Utikal, T.; Götzinger, S.; Sandoghdar, V. Single-Molecule Vacuum Rabi Splitting: Four-Wave Mixing and Optical Switching at the Single-Photon Level. *Phys. Rev. Let.* **2021**, 127(13), 133603.

[46] Daskalakis, K. S.; Maier, S. A.; Kéna-Cohen, S. Polariton Condensation in Organic Semiconductors. *Quantum Plasminics*. Cham: Springer International Publishing. 2017. 151-163.

[47] Agranovich, V. M. "Excitations in Organic Solids." Oxford University Press. 2008.

Supplemental Material

S1. Choosing Electronic Transitions over Vibrational Transitions.

The choice between electronic transitions and vibrational transitions for the molecules was based on many factors. However, one of the main factors was the computational cost of working with vibrational transitions. When comparing electronic transitions in larger organic compounds (like organic dyes in Ref [7]) with vibrational transitions in smaller molecules (like $W(CO)_6$ in Ref [17]), electronic transitions have both greater single molecule dipole moments and greater intermolecular distances. Within a photonic wire configuration, the length in the x direction of the cavity would need to be large enough to maintain the assumptions of the photonic wire. However, with small vibrational molecules having smaller intermolecular distances, the number of molecules needed to reach this length are greater than the number of molecules needed in electronic cases. Thus, to save computational cost, electronic transitions were chosen over vibrational transitions. Future research could incorporate vibrational transitions to compare results with electronic cases.

S2. Infinite-Time Transition Probabilities as a Function of Number of Molecules

In the models generated in this study, there was a simple *1/N* scaling of the infinite-time transition probabilities as a function of the number of molecules. This feature is shown in Figure S1 below.

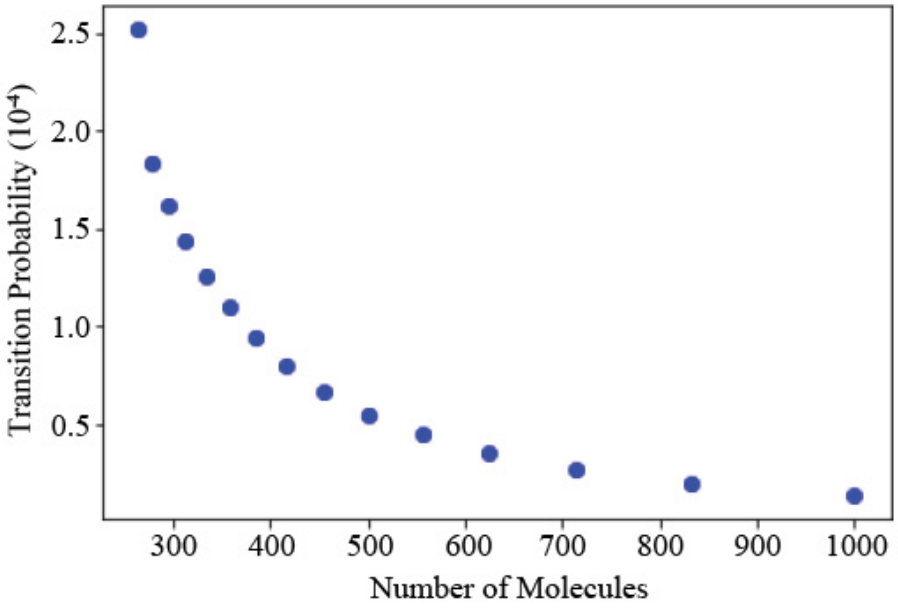

Figure S1. Absolute Infinite-Time Transition Probabilities as a Function of Number of Molecules.

As shown in Figure S1, as the number of molecules increases, the infinite-time transition probability decreases by a factor of approximately *1/N*. This can be attributed to the decrease in single molecule dipole moment as the number of molecules is increased. In all models, the Rabi splitting was kept constant at 0.3 eV. Because the Rabi splitting is proportional to the average single molecule dipole moment multiplied by the number of molecules, as the number of molecules increases, the average single molecule dipole moment must decrease to keep the Rabi splitting constant. This would lower the strength of each molecule's interaction with the cavity.

S3. Transition Probabilities at Different Energetic Disorder Values.

Table S1. Absolute and relative transition probabilities for Figure 6. Relative transition probabilities are relative to the transition probability in the ideal system. Rabi splitting is set at 0.3 eV.

Energetic Disorder as a percent of Rabi Splitting	Absolute Transition Probability	Relative Transition Probability
0.000	5.49166445e-05	1.00000000
0.033	5.63039123e-05	1.02526134
0.066	6.06311504e-05	1.10405781
0.100	6.77771943e-05	1.23418310
0.133	7.80815686e-05	1.42181973
0.166	9.71048427e-05	1.76822243
0.200	1.20476818e-04	2.19381244
0.233	1.62393399e-04	2.95708889
0.266	2.22086711e-04	4.04406921
0.300	3.22948209e-04	5.88069813
0.333	3.69896091e-04	6.73559163
0.366	4.33467427e-04	7.89318851
0.400	4.97563276e-04	9.06033644
0.433	5.89726191e-04	10.73856926
0.466	6.52203405e-04	11.87624281
0.500	6.56747604e-04	11.95899004
0.533	7.36590463e-04	13.41288183
0.566	7.82953980e-04	14.25713437
0.600	7.88330363e-04	14.35503517
0.633	8.51202338e-04	15.49989708
0.666	8.92579519e-04	16.25335138
0.700	9.20926468e-04	16.76953274
0.733	9.30223256e-04	16.93882182
0.766	9.44854616e-04	17.20525033
0.800	9.80124447e-04	17.84749335
0.833	9.61464356e-04	17.50770400
0.866	9.97131348e-04	18.15717907
0.900	9.85878404e-04	17.95226953
0.933	9.88671610e-04	18.00313219
0.966	9.98383820e-04	18.17998585

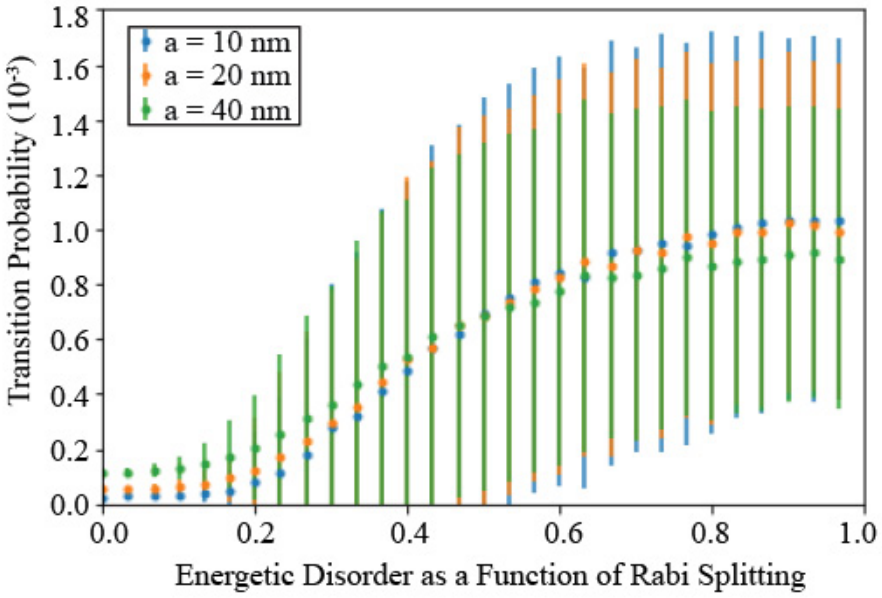

Figure S2. Transition probability as a function of energetic disorder at different intermolecular distances (a). Averages and standard deviations are calculated from 2,500 transition probabilities from 10 different realizations of the Hamiltonian.

S4. Open Quantum System Time Evolution Dynamics

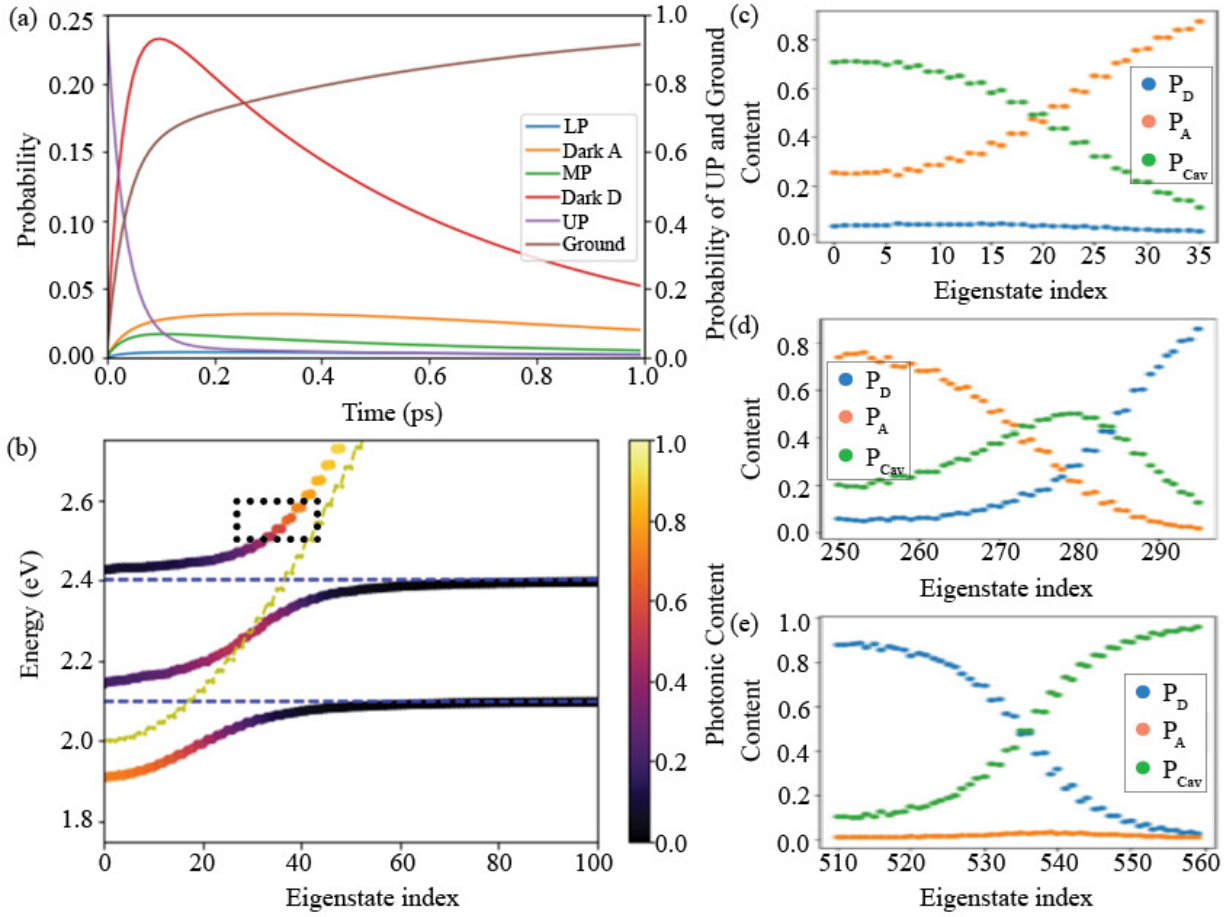

Figure S3. Reproduction of Figure 12. Kinetic observables of an ideal system. Calculations were done using one realization of the Hamiltonian. (a) Time dependent evolution of probabilities within each state. Dark D represents dark donor and Dark A represents dark acceptor. Ground represents the probability that the excitation has decayed via photonic leakage through the cavity or via thermal relaxation through the molecules. (b) Dispersion plot of system. Dotted black rectangular box represents states that were excited. Excitation window was kept between 2.51 and 2.61 eV. (c) (d) (e) Photonic and molecular content of each eigenstate within LP, MP, and UP respectively.

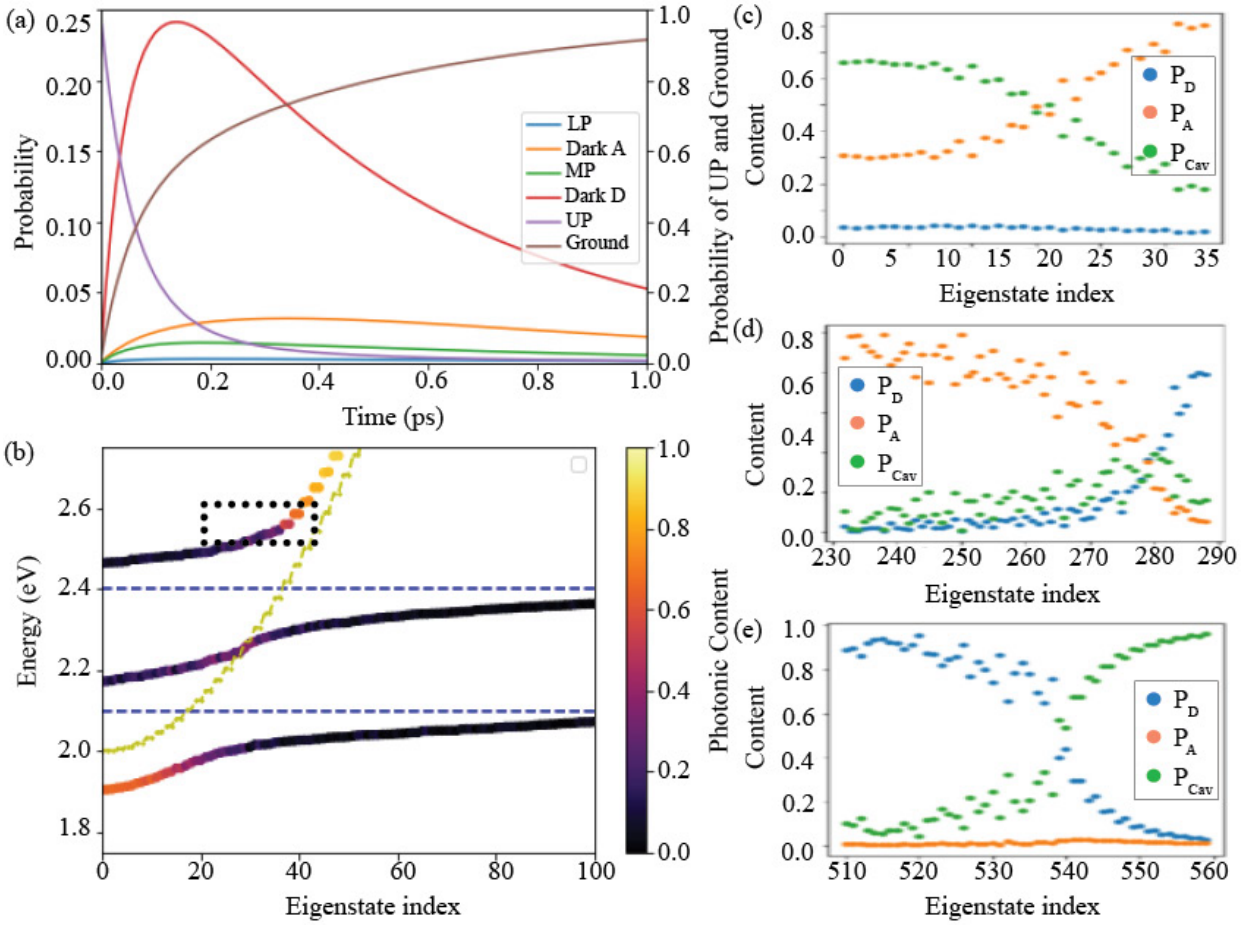

Figure S4. Kinetic observables of a system with 0.015 eV deviation (0.05 times the Rabi splitting) in donor and acceptor excitation energies. Calculations were done using one realization of the Hamiltonian. (a) Time dependent evolution of probabilities within each state. Dark D represents dark donor and Dark A represents dark acceptor. Ground represents the probability that the excitation has decayed via photonic leakage through the cavity or via thermal relaxation through the molecules. (b) Dispersion plot of system. Dotted black rectangular box represents states that were excited. Excitation window was kept between 2.51 and 2.61 eV. (c) (d) (e) Photonic and molecular content of each eigenstate within LP, MP, and UP respectively.

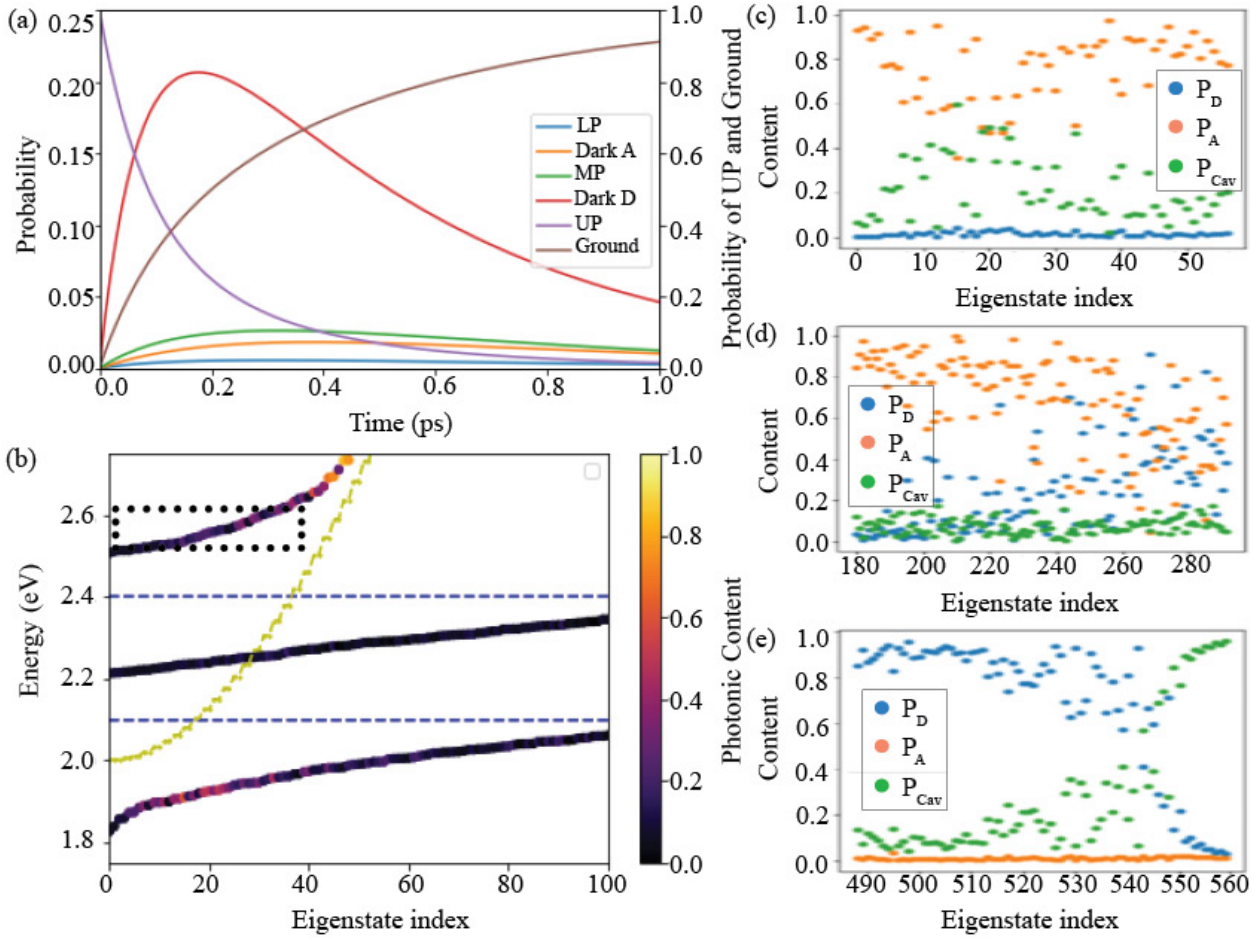

Figure S5. Kinetic observables of a system with 0.03 eV deviation (0.1 times the Rabi splitting) in donor and acceptor excitation energies. Calculations were done using one realization of the Hamiltonian. (a) Time dependent evolution of probabilities within each state. Dark D represents dark donor and Dark A represents dark acceptor. Ground represents the probability that the excitation has decayed via photonic leakage through the cavity or via thermal relaxation through the molecules. (b) Dispersion plot of system. Dotted black rectangular box represents states that were excited. Excitation window was kept between 2.51 and 2.61 eV. (c) (d) (e) Photonic and molecular content of each eigenstate within LP, MP, and UP respectively.

S5. Changes in P_D/P_A Ratio for Different Energetic Disorder

Table S2. P_D/P_A Ratios at initial state and at quasi-equilibrium for an ideal system.

P_D/P_A Ratio at Initial State	P_D/P_A Ratio at Quasi-Equilibrium
17.2297	3.1943
12.3519	3.3274
12.8735	3.3643
8.6666	3.4824
11.4611	3.6463
7.3944	4.8652

*Ratios calculated in Ref [18] were 14 at initial to 2.5 at equilibrium and 25 to 2.6.

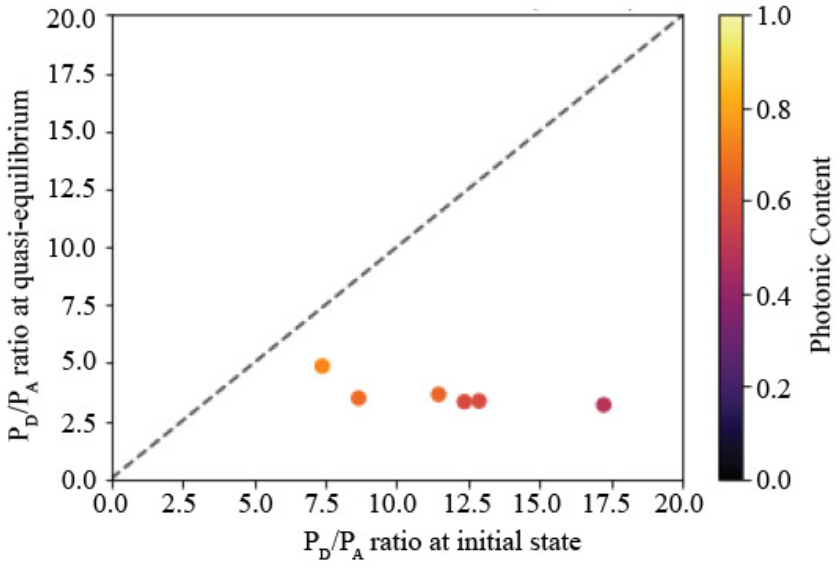

Figure S6. Reproduction of Figure 14. Comparison of P_D/P_A ratio at the initial excited state and the P_D/P_A ratio at quasi-equilibrium for the ideal model. Each point represents one state within the energetic window shown in Figure S2b that was excited. Only one realization of the Hamiltonian was used. Diagonal line is for reference.

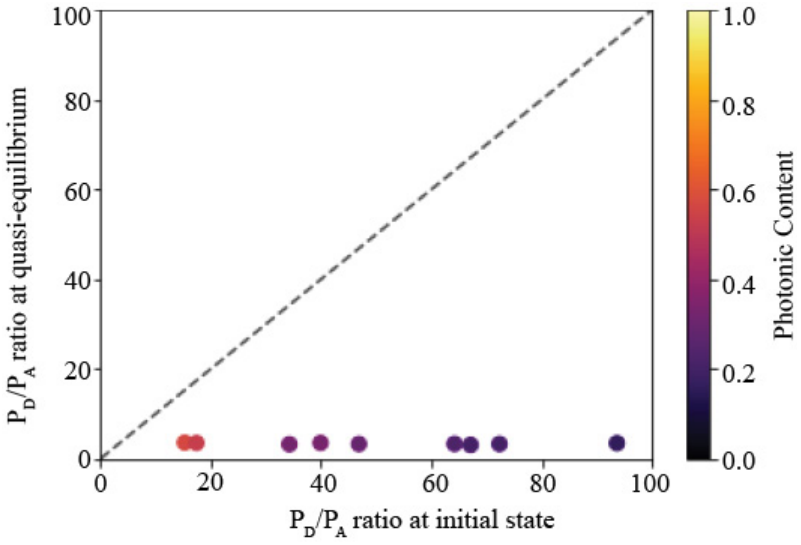

Figure S7. Comparison of P_D/P_A ratio at the initial excited state and the P_D/P_A ratio at quasi-equilibrium for the model with 0.015 eV energetic disorder (0.05 times the Rabi splitting). Each point represents one state within the energetic window shown in Figure S3b that was excited. Only one realization of the Hamiltonian was used. Diagonal line is for reference.

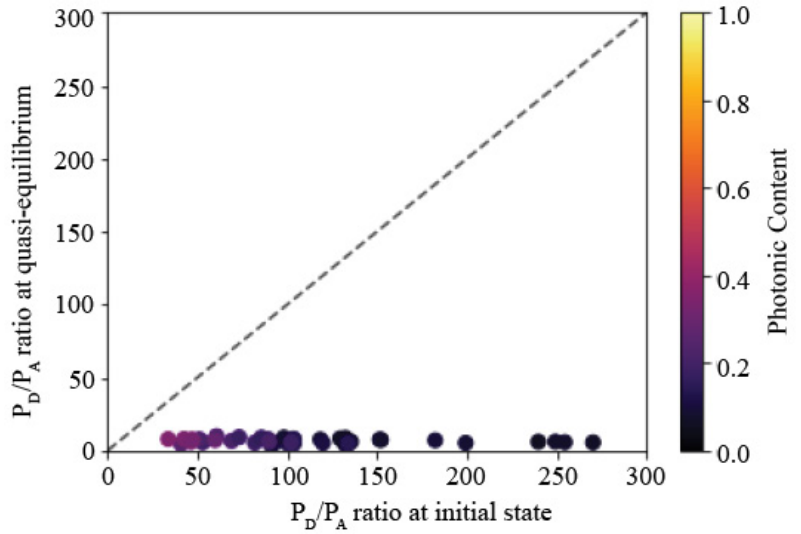

Figure S8. Comparison of P_D/P_A ratio at the initial excited state and the P_D/P_A ratio at quasi-equilibrium for the model with 0.03 eV energetic disorder (0.1 times the Rabi splitting). Each point represents one state within the energetic window shown in Figure S4b that was excited. Only one realization of the Hamiltonian was used. Diagonal line is for reference.

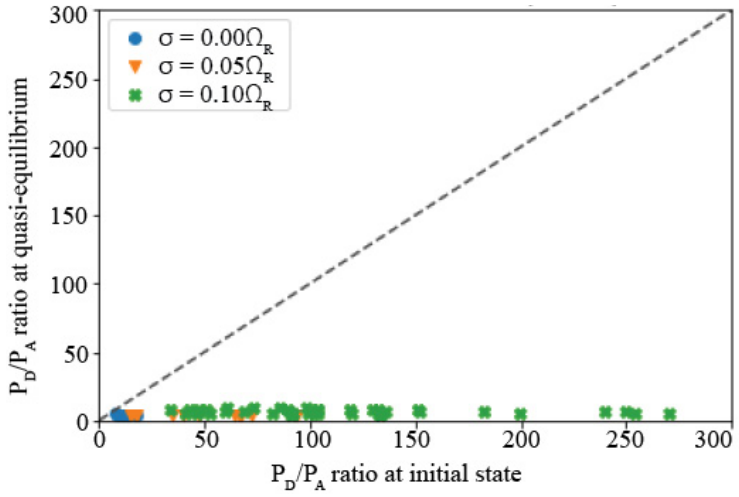

Figure S9. Replication of Figure 15 with diagonal line. Comparison of P_D/P_A ratio at initial excited state and P_D/P_A ratio at quasi-equilibrium for three different energetic disorder (σ) values. Rabi splitting (Ω_R) is set at 0.3 eV. All points are generated using one realization of the Hamiltonian. Diagonal line is for reference.